WRONG SIZE EFFECT IN NaCl-LiCl MIXED CRYSTALS

by
B.T.S.RAMANUJAM

MATERIALS SCIENCE PROGRAMME
INDIAN INSTITUTE OF TECHNOLOGY KANPUR
April, 2000

WRONG SIZE EFFECT IN NaCl-LiCl MIXED CRYSTALS

A Thesis submitted

in partial fulfillment of the requirement

for the Degree of

MASTER OF TECHNOLOGY

by

B.T.S.RAMANUJAM

to the

MATERIALS SCIENCE PROGRAMME

INDIAN INSTITUTE OF TECHNOLOGY, KANPUR

April, 2000

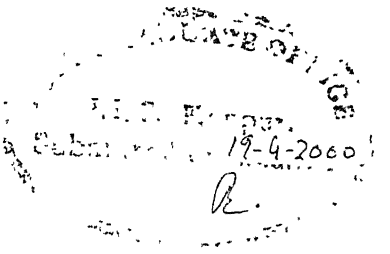

CERTIFICATE

It is certified that the work contained in the thesis entitled, "**Wrong Size Effect in NaCl-LiCl Mixed Crystals**" by B.T.S.Ramanujam, has been carried out under my supervision and that this work has not been submitted elsewhere for a degree.

April,2000

(Keshawa Shahi)

Supervisor

Materials Science Program

I.I.T.Kanpur

ABSTRACT

In the recent past, considerable work has been done on ionic transport processes in solids. Especially, the effect of aliovalent dopants has been extensively studied to understand transport process and to evaluate transport parameters. In all these analysis, the mismatch in size between the dopant ion and the host ion which invariably exists, has been considered negligible and hence neglected. The conductivity of KCl doped with Ca^{2+} and KCl doped with Ba^{2+} with the same concentration of impurities at the same temperature is different which reveals that the difference could only be attributed to the size difference.

Thus, in an attempt to study the effect of size difference between the host and dopant which is termed as " wrong size" and also to obtain conductivity enhancement for material development for various applications, NaCl-LiCl binary system is chosen and studied. It has been found that the relative conductivity of NaCl + 70 m/o LiCl with respect to pure NaCl is ~ 4×10^3 at 560^0C. The mismatch factor defined by $|(r_i/r_h) - 1|$ is ~ 0.3 for this system, where r_h is the ionic radius of the host (Na^+) which is equal to $0.97A^0$ and r_i as that of Li^+ which is equal to $0.68A^0$.

Over all, eleven compositions were prepared and analyzed. Very good correlation can also be found with the phase diagram. Electrical characterization for all samples was done by complex impedance analysis and room temperature XRD for material characterization.

Chapter-1 in this thesis discusses the present problem and the techniques of different types of conductivity enhancement. Chapter-2 details the theory of ionic conduction in solids and mixed crystals Chapter-3 is devoted to experimental and characterization techniques employed. Finally Chapter-4 deals with results and discussion.

ACKNOWLEDGEMENTS

I express my deep sense of gratitude to Professor.K.Shahi, for his consistent and invaluable guidance throughout the course of the present work.

I am greatful to ACMS staff members, for their technical and non-technical assistance in the present work.

I would also thank my labmates Anshuman Dalvi, Debasis Basu, Krishna and Pandeyji for their kind cooperation throughout the course of the present work.

I express my sincere thanks to my class mates, Amit Srivastava, K.K.Manipandey, S.Srikanth, U.D. Saibaba and Mini Grover for their invaluable support throughout my stay at I.I.T.

I am extremely pleased to have friends like, S.Peruncheralathan, P.Vigneshwara Ilavarasan, V. Murali Krishna, Shyam Dhar Dubey, Nagendran, Sankar Rajesh, Sasi, V.Krishnan and Sankaran without whom my stay would not have been more enjoyable one.

Last but not the least, the invaluable support and constant encouragement of my Parents, my Brothers Mr. B.T.S. Raman, Mr. B.T.S. Sampath, my Sister Miss. B.T.S. Thirumamagal and my Athimber can't be expressed in words.

CONTENTS

LIST OF FIGURES

CHAPTER-1

1.1 Introduction

After Faraday propounded the laws of electrolysis, the need of ionic solids, where the charge transport occurs via movement of ions, for practical applications started brewing. Since 1967, a large number of such solids have been discovered and numerous applications found such as solid state batteries, fuel cells etc. The conductivity, which plays a dominant role for their applications in solid state devices paved a path to discover many ionic crystals.

Tubant et al[1] found high ionic conductivity in silver iodide. They discovered that the conductivity of AgI in solid state is almost the same as that in the liquid phase. For practical applications, silver based ionic conductors cannot be used because of their cost unless it is absolutely essential.

The ionic conduction can be explained by the concept of lattice defect or interstitial ions proposed first by Joffe which provided the basis for the successive works of Frenkel and Schottky. An ideal ionic crystal from crystallographic point of view is a non conductor. When an ion receives sufficient energy, it may either jump into other lattice sites or it may be pushed into a near by void space originally not occupied by ions. The first case leads to the formation of Schottky defects and the latter Frenkel defect. These two types of defects are grouped under point defects. The Schottky defects are characterized, e.g., in alkali halides, by equal number of cation and anion vacancies. All silver halides exhibit Frenkel defects like AgCl, β-AgI ($< 147^0$C). These defects are temperature dependent. Generally ionic solids exhibiting Frenkel defects are expected to show high conductivity.

1.2. Types of Ionic Solids

It is natural to classify the ionic solids according to the type of defect or disorder responsible for ionic transport These are principally of two types.

a) Point defect type

b) Molten sublattice type

In the point defect type solids , the transport is through Frenkel or Schottky defect pairs which are thermally generated. The activation energy is generally high, ~ 1eV or more. Point defect type solids can be further subdivided according to the defect concentration density as follows.

c) Dilute : The defect concentration is very low. The number of mobile defects is ~ 10^{18} / cm^3 or less.

examples: AgCl, β-AgI, KCl etc.

d) Concentrated : These contain a large concentration of defects. The defect concentration is ~ 10^{20} / cm^3.

The ionic conductivity of α-AgI[2,3] is due to its unique structure. It has bcc structure in which I^- ions occupy eight corners as well as the body center of the unit cell. The two cations (Ag^+) are distributed over 42 possible interstitial sites per unit cell. Thus the number of cation sites is far greater than the actual number of cations. This situation is referred to a average structure or molten sublattice [4].

Ionic solids can also be classified in to three types according to the magnitude of conductivities.

e) Poor ionic conductors ($\sigma \leq 10^{-6}\ \Omega^{-1}\ cm^{-1}$)

example: Alkali halides

f) Moderate ionic conductors ($10^{-6} \leq \sigma \leq 10^{-3}\ \Omega^{-1}\ cm^{-1}$)

examples: $AgBr$, CaF_2

g) Super ionic conductors ($\sigma \geq 10^{-3}\ \Omega^{-1}\ cm^{-1}$)

examples: α-AgI, $RbAg_4I_5$

Superionic solids are termed "Solid electrolytes" or "Fast ion conductors". The ionic conductivity varies vastly with temperature and also from one solid to the other. The highest conductivity[5] at room temperature obtained so far is $0.27\ \Omega^{-1}\ cm^{-1}$ for $RbAg_4I_5$ whereas for normal ionic solids like NaCl, KCl etc., the room temperature conductivity $\sim 10^{-12} - 10^{-16}\ \Omega^{-1}\ cm^{-1}$.

The conductivity of any ionic solid is a product of two exponential functions as given below.

$$\sigma = n(T)\ \mu(T)\ e = A \exp(-H / 2kT) \exp(-h / kT)$$

where n is the concentration and μ the mobility of a particular type of defect, A is the pre-exponential term which includes charge of the conducting species, H and h are the formation and migration enthalpies respectively. The conductivity (σ) is also related to the diffusion constant D through the Nernst - Einstein relation

$$\sigma = n e^2 D / kT$$

where e is the charge of the conducting ion.

It should be emphasized here that the conductivity (σ) depends mainly on the defect concentration n(T) rather than on the mobility $\mu(T)$. The mobility [(6)] for all normal salts lies in the range 10^{-4}-$10^{-6}\ cm^2\ V^{-1}\ s^{-1}$.

Table 1: Conductivity of some ionic crystals[6]

Material	Conductivity σ (Ω^{-1} cm^{-1}) at T_m ^0C	Melting Temperature T_m (°C)
LiCl (sc)	9×10^{-3}	606
LiI (sc)	5×10^{-2}	452
NaCl (sc)	1×10^{-3}	800
NaI (pc)	2.1×10^{-3}	661
RbCl (sc)	1.3×10^{-5}	717
CsCl(α) (sc)	6.1×10^{-5}	636
CsI (sc)	1.9×10^{-3}	621

sc - single crystal

pc - poly crystal

Solid electrolytes are of different types based on structure.

1. Crystalline solid electrolytes.
2. Amorphous solid electrolytes.
3. Polymer solid electrolytes.
4. Composite solid electrolytes.

They can also be classified according to the type of charge carriers.

1.3 Need for Efficient Solid Electrolytes

Eventhough silver based solid electrolytes have high conductivity, from practical application point of view they can't be used because they are not cost effective. So there is need for search of materials which are economical and easily available These materials may not exhibit a high conductivity e.g., alkali halides, but it is always possible to enhance their conductivity. There are several possible techniques which can be employed for this purpose.

a) Dispersion of fine insulating particles like Al_2O_3, SiO_2 etc.

b) Aliovalent doping

c) Homovalent doping

Liang[7] discovered that the dispersion of fine insulating alumina particles in LiI enhances the Li^+ ion conductivity considerably. Following this work considerable progress has been made[8,9] in this field. The conductivity enhancement in such composites according to Jow and Wagner[10] is because of the formation of space charge layer. In the bulk of the crystal, an individual component of a defect pair cannot be created without simultaneously creating the other charge compensating component. However, it could be formed separately at the heterogeneity such as free surfaces and matrix - particle interfaces. Their model could predict the conductivity enhancement with the size of the dispersoid (inversely related) but fails to predict the composition corresponding to the maximum conductivity.

1.3.1 Aliovalent doping

An impurity ion whose valency is different from that of the corresponding host ion is referred to as aliovalent ion. Thus when alkali halides are doped with

divalent cations or anions, from charge neutrality principle, the excess defects of compensating type will be generated leading to increase in conductivity.

1.3.2 Homovalent doping

Substitution of ions having the same valency as the corresponding host ion also has a tremendous effect on conductivity. The enhancement in conductivity depends on the concentration and the relative size of the dopants. There always exists a size difference between the dopant and the host and larger the mismatch factor, $\delta = |(r_i / r_h) - 1|$, where r_i and r_h are ionic radii of the impurity (dopant) and the host ions respectively, higher is the enhancement in conductivity.

The conductivity of $LiI_{0.75}Br_{0.25}$ was found to be $\sim 5 \times 10^{-7}$ $\Omega^{-1}cm^{-1}$ at 293^0K, which is higher than the pure components (Table 2) at the same temperature. Apart from the conductivity enhancement, the homovalent dopants (Table 2) are found to decrease the transition temperature as observed by Shahi and Wagner in βAgI - AgBr mixed crystals. The same effect was observed by Ihara et al (Table 2) in $AgI_{1-x}Cl_x$ ($0 < x < 0.1$) in the temperature range 60 - 200^0C. The effect of Cl^- ions is more pronounced than that of Br^- ions because of larger mismatch in case of the former. For various other mixed crystals studied so far, the conductivity enhancement is shown in Table 2. An inspection of this data will reveal the fact that for a particular composition of dopant, the conductivity attains a maximum value. This is consistent with the phase diagram which exibits a minimum for that composition, implying the maximum possibility of increment in defect concentration at any temperature.

Table 2. The electrical conductivity (σ_x) and the relative conductivity (σ_x / σ_0, σ_0 being the conductivity of pure component) at a fixed temperature T (^{0}C) of some selected mixed crystals.

Mixed crystals	Conductivity σ_x (Ω^{-1} cm^{-1})	σ_x / σ_0	Temperature (^{0}C)
KCl + 70 m/o RbCl [11]	5.5×10^{-5}	5	660
KBr + 50 m/o KI [12]	2.9×10^{-4}	63	500
LiBr + 40 m/o LiI [13]	1.8×10^{-6}	34	385
NaCl + 47 m/o NaBr [14]	8.0×10^{-5}	10	393
CsCl + 70 m/o TlCl [15]	5.6×10^{-2}	7×10^3	387
AgI + 4 m/o AgBr [16]	4.3×10^{-6}	16	25
AgBr + 30 m/o AgI [17]	6.5×10^{-6}	77	25
AgI + 10 m/o AgCl [18]	7.9×10^{-5}	125	25
LiBr + 75 m/o LiI [19]	5.0×10^{-7}	80	25
KCl + 50 m/o NaCl[20]	8.0×10^{-6}	80	500
KBr + 70 m/o NaI[21]	2.5×10^{-4}	500	500

A semi quantitative model, viz., lattice loosening model[17], explains the transport properties in mixed crystals. Since the host and the dopant ions have the same valence, classical doping concept cannot be used to explain the observed enhancement in σ. Shahi and Wagner[17] have argued that both the concentration and mobility of the defects affect the enhancement in conductivity. According to the lattice loosening model, the substitution of the homovalent ions which are either larger or smaller than the host ions, usually leads to a decrease in the melting temperature as supported by phase diagrams and hence in formation and migration energies of the defects.

The role of wrong size (mismatch factor, δ) can be further gauged from the following observations; The conductivity enhancement in KCl - KBr with a low mismatch factor of ~ 8 % is only by a factor of 2, whereas in CsCl - 70 m/o TlCl with a higher mismatch factor of ~ 13 % , the enhancement in σ is ~ 7×10^3 at 387^0C. Hence it is desirable to study the effect of wrong size substitutions on the ionic transport in mixed crystal systems. The substitution of too large or too small ions might cause the host ions around the dopant to readjust in order to allow the dissolution. Thus the elastic displacement so produced is likely to weaken the bonding between the atoms or cause lattice loosening.

1.4. Motivation and Scope of present investigation

Most of the known superionic solids are silver based which are not cost effective. Therefore, it may be desirable to explore the possibility of enhancing the conductiviy of so called normal ionic solid so that they may be used as a substitute. With this motivation, one such alkali halide mixed crystal system namely NaCl - LiCl is chosen for the present work. Apart from this, this binary system exhibits both solid

solution as well as two phase mixture region and the two alkali halides do not undergo any solid - solid phase transition. Thus the aim of the present work may be stated as below.

1) To study the effect of homovalent dopant namely LiCl on the ionic transport properties of NaCl.

2) To show the effect of wrong size of the dopant and the host (size mismatch) on the conductivity.

3) To show that the conductivity enhancement can be had at low temperatures itself because of precipitation of second phase particles during cooling cycle, and

4) To test the validity of lattice loosening model developed for mixed crystals.

CHAPTER- 2

THEORETICAL ASPECTS

Impurities play a dominant role especially in the electrical transport properties of solids. These are called structure sensitive properties. Ionic conductivity and diffusivity are structure sensitive properties. As pointed out in the previous Chapter an ideal ionic crystal, from crystallographic point of view, is an insulator. However in real crystals such as alkali halides, there are lattice points which are not actually occupied or atoms that are placed at sites which are not the regular lattice point (e.g. AgCl). The former is called vacancy and the latter an interstitial atom. These imperfections are called point defects or zero dimensional defects to distinguish them from other types of defects such as dislocations and used to explain ionic transport processes in solids such as alkali halides. Therefore, an understanding of the concept of point defects is essential to explain ionic transport in alkali and silver halides.

2.1 Schottky defects

During diffusion and conduction, ions must move through the lattice by some jumping process. This is achieved by defect formation. When the vacancies are created by pushing the ions to external surface(s), these are called Schottky vacancies. In monovalent salt like NaCl, equal number of cation and anion vacancies are formed to preserve electrical neutrality of the solid. The production of Schottky defects in alkali halides (MX) can be represented by the following reaction

$$\text{crystal (MX)} \leftrightarrow V_M^{'} + V_X^{\cdot}$$

where Kroger's notation is used.

V_M - vacancy at the cation site which has negative charge denoted by ($'$)

V_X - vacancy at the anion site denoted by (.)

Thus the production of Schottky defects can be envisaged as the removal of a cation and an anion from the interior to the surface of the crystal, leaving a cation and an anion vacancy. This process requires energy and also allows an increase in configurational entropy. The configurational entropy is given by

$$S_{cf} = k \log [(N+n)! / N!\, n!]^2 \qquad (2.1)$$

The term in square brackets represents the number of ways in which N positive ions and n positive ion vacancies may be distributed over a total of (N+n) sites. The same holds for the negative ion sites, hence the square. If the energy H_+ required to produce a single positive ion vacancy which is different from the energy H_- to produce a single negative ion vacancy, they would occur approximately in equal numbers in the interior of the crystal as pointed out earlier. It is obvious from this that their number will be determined only by the sum of the formation energies

$$H = H_+ + H_- \qquad (2.2)$$

The equilibrium condition requires the free energy H-TS to be minimum. The free energy of a fictitious perfect crystal will be represented by

$$G_p = H_p - TS_p \qquad (2.3)$$

where H_p incorporates the binding energy as well as the vibrational energy. The entropy is thermal entropy only because for a perfect crystal the configurational entropy vanishes. Let the actual crystal contains n positive and n negative ion vacancies. Its configurational entropy is given by Eq.2.1. The free energy change between the actual crystal perfect crystal may thus be represented by

$$\Delta G = nH - T(S_a - S_p) - 2kT \log[(N+n)!/ N!n!] \qquad (2.4)$$

where S_a is the thermal entropy of the actual crystal. Let us define the increase in thermal entropy ΔS_{th} resulting from the production of a positive plus a negative ion vacancy by

$$n \Delta S_{th} = S_a - S_p \qquad (2.5)$$

when $S_p = 0$; $\Delta S_{th} = S_a / n = S$

Thus Eq.2.4 can be written as

$$\Delta G = nH - nTS - 2kT \log [(N + n)! / N! n!]$$

$$= n [H - TS] - 2kT \log [(N + n) / N! n!]$$

$$= ng_s - 2kT \log [(N + n) / N! n!] \qquad (2.6)$$

where g_s represents the free energy of formation of a single Schottky pair and is given by

$$g_s = H_s - TS_s \qquad (2.7)$$

The subscript s represents Schottky defect.

Applying equilibrium condition $(\partial \Delta G / \partial n)_T = 0$, we obtain for $n << N$

$$n = N \exp (- g_s / 2kT) \qquad (2.8)$$

It is convenient to write n_c for concentration of cation vacancies and n_a for anion vacancies. From Eq. 2.7, one can write,

$$n_c = n_a = N \exp (S_s/2k) \exp (-H_s/2kT) \qquad (2.9)$$

where H_s is the enthalpy of formation of a Schottky defect and S_s corresponding entropy of formation of the same. Equation (2.9) is often considered to be an expression of law of mass action, i.e., the product of the concentration of anion vacancies and of cation vacancies is a constant.

2.2 Frenkel defects

When a vacancy is created by pushing the atom in to the interstitial site, such vacancy - interstitial pairs are called Frenkel defects. In MX type solids such as silver halides, the formation of Frenkel defect is expressed as

$$\text{crystal} \leftrightarrow V_M^{'} + M_i^{\cdot}$$

V_M refers to the negatively charged vacancy at the cation site and M_i denotes the M ion (cation) with an effective positive charge denoted by the superscript located at an interstitial site. The expression for the concentration defects, neglecting thermal entropy changes

$$n = (NNi)^{1/2} \exp (- g_f / 2kT) \qquad (2.10)$$

where N is the number of cations (or anions) under consideration and N_i the number of possible interstitial sites in the crystal and g_f is the free energy of formation of a Frenkel defect pair.

2.3 Mobility and Ionic conductivity

The ion transport is governed by the jump probability of the mobile ion which is proportional to

1) The probability for the ion to jump in to the defect in a given direction in unit time, which is the jump frequency ω.

2) the probability that a given site has a defect on a nearest neighbor site. This is the mole fraction of defects multiplied by the number of nearest neighbour sites.

The jump frequency depends on the potential barrier seen by the ions. Assuming Einstein model to be true and that the ions are vibrating harmonically around their equilibrium position with a vibrational frequency ν_0. Expression for the jump frequency for a point defect in ionic solids has been derived and it is given by,

$$\omega = \nu_0 \exp (- g_m / kT) \quad (2.11)$$

where g_m is the free energy barrier that opposes the migration of the ion and is termed the free energy of migration g_m can be written as

$$g_m = h_m - Ts_m \quad (2.12)$$

where h_m is the enthalpy of migration and s_m is the entropy of migration. Hence,

$$\omega = \nu_0 \exp (s_m / k) \exp (- h_m / kT) \quad (2.13)$$

The above expression is for the thermodynamic equilibrium allowing an equal number of jumps in both directions. When an electric field is applied, the potential barrier is seen by an interstitial ion jumping from one position to the other. Therefore an additional term -qEx is added to the potential energy term where 'q' is assumed to be the charge on the interstitial ion. The subsequent saddle point energy keeps on decreasing by an amount qaE/2 (x=a/2, where 'a'is the inter atomic distance). A jump in the field direction with a greater probability is given by

$$\omega' = \nu_0 \exp [-(g_m - qaE/2)/ kT] \quad (2.14)$$

and a jump against the field direction takes place with reduced probability.

$$\omega'' = \nu_0 \exp [-(g_m + qaE/2)/kT] \quad (2.15)$$

The net number of ions moving per unit volume in the direction of field

$$n' = n (\omega' - \omega'') \approx n\omega qaE / kT \quad (2.16)$$

assuming qaE << kT. Here 'n' is the number of interstitial ions per unit volume. Thus the current density 'j' (amount of charges passing per unit area per unit time) is given by

$$j = na^2q^2\omega E / kT \quad (2.17)$$

The ionic conductivity is given by

$$\sigma = j / E = na^2q^2\omega / kT = nq\mu$$

where the mobility μ is given by

$$\mu = a^2 q\omega/kT \qquad (2.18)$$

In NaCl type solids the charge carrier has to jump a distance 2a in the field direction. Hence the mobility term will contain an additional factor 4.

$$\mu = 4a^2 q\omega / kT \qquad (2.19)$$

The ionic conductivity of solids having rocksalt structure in which the dominant type of defects are cation and anion vacancies,

$$\sigma = q (n_c \mu_c + n_a \mu_a) \qquad (2.20)$$

substituting for n_c, μ_c and μ_a from (2.9), (2.18) one obtains the conductivity

$$\sigma = 4Nq^2a^2/kT [\nu_c \exp (S_s/2k + s_{mc} / k) \exp (-(H_s/2 + h_{mc})/ kT)$$

$$+ 4Nq^2a^2/kT [\nu_a \exp (S_s / 2k + s_{ma} / k) \exp (-(H_s/2 + h_{ma}) / kT)] \qquad (2.21)$$

where 'q' is the charge and the subscripts s, m, c and a refer to Schottky type, migration, cation vacancy and anion vacancy. The above equation can be simplified as

$$\sigma T = A_c \exp (- E_{ac}/kT) + A_a \exp (- E_{aa}/kT) \qquad (2.22)$$

where $E_{ac} = H_s / 2 + h_{mc}$ and $E_{aa} = H_s/2 + h_{ma}$

the term h_m refers to the enthalpy of migration of defects. Entropy terms are included in the preexponential factor.

Thus the conductivity equation becomes more complex when more than one type of defects participate in the conduction mechanism. But in reality, for most ionic solids specifically alkali halides, the contribution of one type of defect is more than the other which is often neglected. Thus equation (2.22) can be written in general as

$$\sigma T = A \exp (-E_a/kT) \qquad (2.23)$$

E_a is known to be the over all activation energy comprising of half the enthalpy of formation and the enthalpy of migration of defects.

2.4 Defect Concentration in Pure Ionic Crystals

For the case of Schottky defects, if the mole fraction of positive and negative ion vacancies respectively be x_c and x_a and their respective numbers be n_c and n_a, then

$$n_c = n_a = N \exp (- g_s / kT) \quad (2.24)$$

$$x_c x_a = x_0^2 = \exp (- g_s / kT) = \exp (S_s / k) \exp (-H_s / kT) \quad (2.25)$$

where g_s, S_s, H_s are the Gibbs free energy, entropy and enthalpy of formation respectively of a Schottky pair. N is the number of cation or anion sites.

In the case of pure crystal, the charge neutrality condition is written as

$$x_c = x_a = x_0 \quad (2.26)$$

2.4.1 In Doped Crystal

When an ionic crystal is doped with aliovalent impurity like Ca^{2+}, excess of cation vacancies will be created to compensate for the charge difference. The charge neutrality condition demands that

$$x_c = c + x_a \quad (2.27)$$

where c is the mole fraction of divalent cation impurity added. From (2.27), (2.24)and (2.25) one can get

$$x_a = c/2 \{ [1 + (2x_0/c)^2]^{1/2} + 1 \} \quad (2.28)$$

$$x_c = c/2 \{ [1 + (2x_0/c)^2]^{1/2} - 1 \} \quad (2.29)$$

For larger dopant concentration, $c >> x_0$

$$x_a = c$$

$$x_c = x_0^2/c$$

For small dopant concentrations ($c << x_0$), the concentrations x_a and x_c reduce to the pure crystal values as expected. i.e., $x_c = x_a = x_0$. One can also get similar expressions when the crystal is doped by a divalent anion impurity like carbonate, sulphate ions with a concentration c_1. The charge neutrality condition can be written as

$$x_c + c_1 = x_a$$

The values of x_a, x_c in this case will be

$$x_a = c_1/2 \{ [1 + (2x_0/c_1)^2]^{1/2} + 1\} \quad (2.30)$$

$$x_c = c_1/2 \{ [1 + (2x_0/c_1)^2]^{1/2} - 1\} \quad (2.31)$$

2.5. Estimation of Transport Parameter

From equation (2.23), it can be seen that the conductivity expression contains the overall activation energy. The plot of log (σT) vs 1/T is linear whose slope yields the overall activation energy E_a. However since the variation of logT over the experimental range is negligible in comparison to that of logσ. A plot of log σ vs 1/T is also found to be linear and it is preferred because of its simplicity. However the activation energy E_a obtained from this plot is slightly lower than the actual value by an amount equal to the thermal energy kT.

Generally a plot of logσ vs 1/T for a nominally pure ionic solid consists of two linear segments; a high temperature linear region which shows the intrinsic properties of the material and a low temperature extrinsic region characterized by a lower slope and hence lower activation energy. The intrinsic region relates to the temperature range in which the dominant defects are those which are present due to thermodynamic considerations. In this case E_a is the sum of half the formation energy and migration energy of defects. The extrinsic region arises because of impurities. In this region E_a is simply the migration energy alone. The extrinsic - intrinsic transition

temperature is known as knee temperature and is often used as a measure of impurity level in the crystal. The complete conductivity curve (log σ vs 1/T) is therefore generally a superposition of two linear segments corresponding to

1) $A_1 \exp (- E_1 / kT)$ in the low temperature, extrinsic region.

2) $A_2 \exp (-E_2 / kT)$ in the high temperature, intrinsic region.

The activation energy E_1 is less than E_2. The pre-exponential factor A_2 is independent on the purity of the material while A_1 increases as the impurity of the specimen increases in the sample.

Theory of Ionic Conduction In Mixed Crystals

2.6 Concentration of defects in mixed crystals

When the charge of the host and the dopant ion is the same, classical doping concept cannot be used to explain the observed conductivity enhancement. However, in mixed crystals a semi-quantitative lattice loosening model is used to account for the enhanced conductivity. This was proposed by Shahi and Wagner[12] and has since been tested on several system in KBr - KI[22], KCl - KBr[23], NaBr - NaI[24], NaBr - LiBr[24], KBr - NaI[21], KBr - NaBr[25], AgBr - AgI[17] etc.

The above model states that the substitution of either too large or too small ion generally introduces strain in the host lattice and hence weakens the bonding and eventually results in the lowering of melting point of the mixed crystal. Phase diagram of many mixed crystal system will prove the above argument. One can observe a clear minimum in the phase diagram for a particular composition, suggesting the validity of lattice loosening model. Thus the formation enthalpy of defects corresponding to that composition is minimum and hence conductivity should be maximum.

A semi quantitative expression for the concentration of point defects in mixed crystal can be arrived in view of the existing good empirical correlation between the enthalpy of formation (H_s) of Schottky defects and the melting temperature (T_m) of ionic solids. According to Barr and Lidiard[26], H_s and T_m are linearly related as

$$H_s = \alpha T_m \tag{2.32}$$

where α is the proportionality constant and has a value of 2.14×10^{-3} eV/k. The above equation for mixed crystal can be written as

$$H_{sx} = \alpha T_{mx} \tag{2.33}$$

$$(H_{sx} - H_{so}) = \alpha (T_{mx} - T_{mo}) \tag{2.34}$$

$$\Delta H_{sx} = \alpha \Delta T_{mx}$$

where H_{sx} refers to enthalpy of formation of defects in mixed crystals and H_{so} as that of the pure crystal. Similarly T_{mx} represents the melting temperature of mixed crystals and T_{mo} as that of the pure component.

The expression for the concentration of Schottky defects for mixed crystals can be written as

$$n_x = A_x \exp [-H_x/ (2kT)] \tag{2.35}$$

where A_x is the pre-exponential factor. The ratio of the concentration of Schottky defects in the mixed crystal to that in the pure crystal is given by

$$n_x/n_0 = (A_x/A_o) \exp [-(H_x - H_o) / (2kT)] \tag{2.36}$$

From Eqn.2.34, Eqn. 2.36 becomes,

$$n_x/n_0 = A_x/A_0 \exp [- \alpha \Delta T_{mx} / (2kT)] \tag{2.37}$$

The concentration of defects in mixed crystal relative to that of pure component is ingeneral depends on ΔT_{mx} of the mixed crystal, provided the ratio of the pre-exponential factors can be calculated.

$$A_x/A_0 = \exp [(S_x - S_0) / (2k)] \quad (2.38)$$

The entropies of formation of defects in mixed crystal and in pure crystal in general will not be different and hence their difference is negligible. Thus A_x/A_0 can be taken as unity. Thus

$$n_x/n_0 = \exp [-\alpha \Delta T_{mx} / (2kT)]$$

The above equation represents the relative concentration of vacancies as a function of the change in the melting point (ΔT_{mx}) of the mixed crystal. Since the melting temperature of the mixed crystal is less than that of the pure component, ΔT_m is negative and hence predicts an enhanced concentration of defects.

In mixed crystals, mobility of ions increases. A very good correlation between the enthalpy of migration of defects and the melting temperature was given by Barr and Lidiard[27]

$$h_m = \beta T_m - \gamma \quad (2.39)$$

where β is a constant ($= 0.84 \times 10^{-3}$ eV/k) and also $\gamma = 0.2$ eV. For mixed crystals, the enthalpy of migration of defects

$$h_{mx} = \beta T_{mx} - \gamma \quad (2.40)$$

and for pure crystal

$$h_{mo} = \beta T_{mo} - \gamma \quad (2.41)$$

$$h_{mx} - h_{mo} = \beta (T_{mx} - T_{mo})$$

$$\Delta h_{mx} = \beta \Delta T_{mx} \quad (2.42)$$

The ratio of mobility of cation vacancies in mixed crystal to that of the pure crystal

$$\mu_x / \mu_0 = \exp [-(h_{mx} - h_{mo}) / (kT)] \quad (2.43)$$

Taking the ratio of preexponential factor to be unity, from (2.42), (2.43) becomes

$$\mu_x / \mu_0 = \exp [- \beta \Delta T_m / (kT)] \quad (2\ 44)$$

The ratio of the mobility of cation to that of anion vacancies in the mixed crystals remain almost the same as that in the component crystals over the entire compositional range Thus if the cation vacancies are more mobile, then the ionic conductivity in mixed crystals is related to that of the pure component by the following expression

$$\sigma_x / \sigma_0 = (n_x \mu_x) / (n_0 \mu_0)$$

$$= \exp [- (\alpha/2 + \beta) \Delta T_{mx} / (k T)] \qquad (2.45)$$

On substituting for α,β and k= 8 6 $\times 10^{-5}$ eV/k, the above equation becomes,

$$\sigma_x / \sigma_0 = \exp (- 22\ 17 \times \Delta T_{mx} / T) \qquad (2.46)$$

The above expression is based on the lattice loosening model and the empirical correlations expresses the enhancement in σ_x of the mixed crystals relative to that of the pure crystal (σ_0) as a function of the change in the melting temperature due to the substitution of homovalent dopants.

CHAPTER-3

EXPERIMENTAL DETAILS AND CHARACTERIZATION TECHNIQUES

a) Experimental Details

3.1 Sample Preparation

Starting materials LiCl (purity > 99%) and NaCl (purity > 99%) were obtained from Aldrich Chemicals Inc. USA

Physical Properties of LiCl

Molecular weight : 42.39

Bravais Lattice : fcc

Density : 2.068 g/cc

Melting Point : 605^{0}C

Boiling Point : 1325-1360^{0}C

Physical Properties of NaCl

Molecular Weight : 58.44

Bravais Lattice : fcc

Density : 2.165 g/cc

Melting Point : 801^{0}C

Boiling Point : 1413^{0}C

The starting materials, LiCl and NaCl were kept inside a dry box containing P_2O_5 to absorb any moisture present inside the dry box as both of them (especially LiCl) are very hygroscopic and thus under no circumstances these were exposed to the atmosphere. Mixed crystals of different compositions were prepared by weighing appropriate amounts of LiCl and NaCl. To avoid absorption of water during weighing an arbitrary amount of LiCl was weighed first and accordingly the appropriate proportion of NaCl was calculated and weighed In this way long exposure of LiCl during weighing was reduced These materials were then transferred to a mortar which was cleaned with acetone and preheated to ~120^{0}C and kept inside an oven. The mixture was ground inside the oven itself in presence of P_2O_5, transferred into an alumina crucible which was immediately shifted to a furnace preheated to ~ 200^{0}C. The temperature of the furnace was raised above the melting point of the mixture and after allowing five minutes for homogenization, the furnace was switched off. When the furnace cooled to ~ 100^{0}C, the resolidified material was transferred in to a mortar and ground well inside the oven for further homogenization. A steel die was also preheated and a small amount of the material was transferred in to it and the die was wrapped in a plastic bag and then pellets were made, of diameter 11mm. The pellets were then sintered at appropriate temperatures, given in the Table 3, for sufficiently long time ($\geq$ 9 hrs) and then graphite paint electrode was applied on to the two flat surfaces of the sintered pellets and dried. These pellets were then loaded in the sample holder and their impedances measured in the cooling cycle using 4192A Impedance Analyzer. Chromel-alumel thermocouple was used to measure the temperature of the sample inside the furnace.

Table 3. Sintering Temperature, Sintering time and thickness of different samples prepared.

Pelletization Pressure: 6 ton/cm^2

Composition	Sintering Temperature (^{0}C)	Time (hrs)	Thickness Of The Pellet (cm)
NaCl (Pure)	700	18	0.280
NaCl + 10 m/o LiCl	629	16	0.264
NaCl + 20 m/o LiCl	583	20	0.440
NaCl + 30 m/o LiCl	575	13	0.250
NaCl + 40 m/o LiCl	527	24	0.300
NaCl + 50 m/o LiCl	509	17	0.414
NaCl + 60 m/o LiCl	483	11	0.394
NaCl + 70 m/o LiCl	432	16	0.362
NaCl + 80 m/o LiCl	421	20	0.472
NaCl + 90 m/o LiCl	502	20	0.390
LiCl (Pure)	484	10	0.362

3.2 Sample Holder

Fig.3.1 shows the schematic diagram of the sample holder. It consists of three identical lava discs (diameter ~ 2.5 cm and thickness ~ 1cm), each having a central hole and four symmetrically located holes near the periphery. The lava discs, after machining were heated slowly to 1000^{0}C and kept at that temperature for two hours to harden them. A pair of stainless steel rods were passed through the two diametrically opposite holes to provide support to the sample holder The spring which

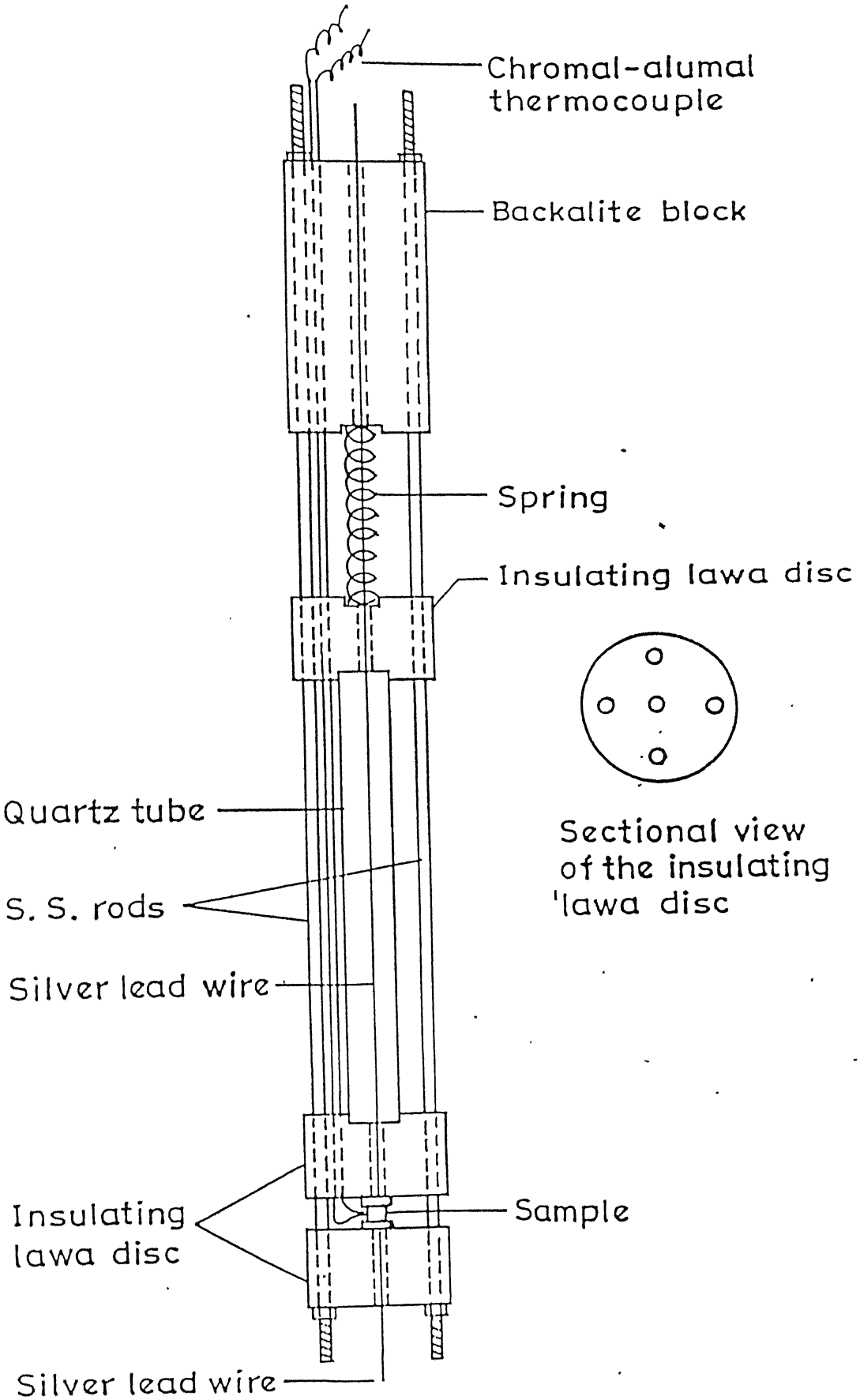

Fig.3.1. Sample holder for electrical conductivity measurement from room temperature to 1000°C

was so located that it remains outside the furnace. The spring provides a firm contact between the electrodes and the sample holder. The flat surfaces of the cylindrical pellets were polished to remove surface contamination and to obtain smooth surface. The pellets were carefully placed between the two silver electrodes.

3.3 Furnace and Temperature Controller

An electrical resistance heating furnace comprising of a mullite tube (diameter ~ 1.5 inches) over which kanthol wire was wound uniformly has been used. The resistance of the heating element was ~ 50 ohm. A high temperature cement was applied over the kanthol winding to fix them in place. The mullite tube with cemented kanthol wiring was enveloped with a cylindrical stainless steel container and the space between the two shells was filled with MgO powder to minimize the heat loss.

The temperature inside the furnace was measured using a chromel-alumel thermocouple. A PID type temperature controller (Indotherm, model 401D) was used to control the furnace temperature. The temperature was controlled to within $\pm 1^{0}C$

3.4 Impedance Analyzer

Fig.3.2 shows the block diagram of the impedance analyzer. HP 4192A impedance analyzer along with HP1607A test fixture has been employed for complex impedance measurements. The equipment has an auto balancing bridge with a test signal from 5mV to 1.1V. It has a built in frequency synthesizer which has a frequency range 5 Hz - 13 MHz. There are two display sections namely display A and display B which provided direct read out of the selected measurement parameters.

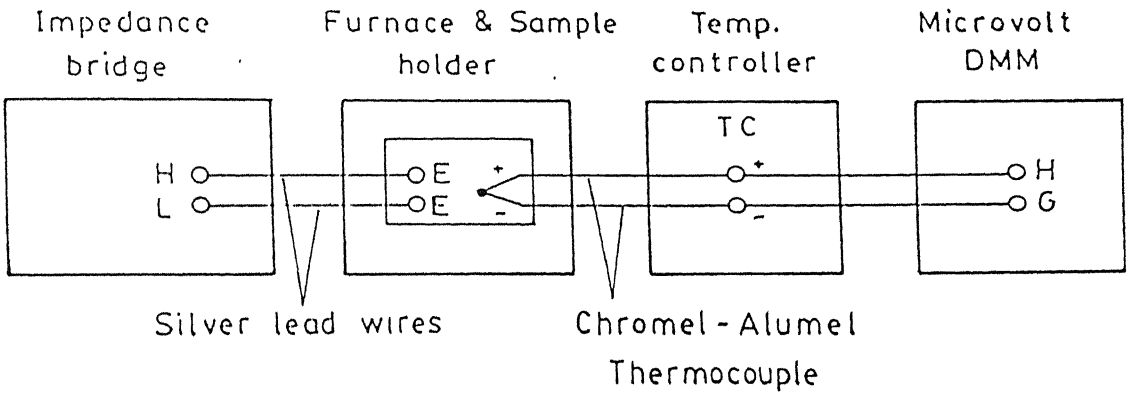

Fig.3.2. Block diagram connections for electrical conductivity measurements

3.5 X-Ray Diffraction

X-ray diffraction patterns of various compositions have been recorded using a Richeifert (Iso-Debyeflex 2002D) counter diffractometer employing a filtered CuK_α radiation ($\lambda = 1.542A^0$). The generator was operated at 30KV and 20mA. The scanning speed was 3^0 per minute in 2θ. All XRD patterns were recorded at room temperature.

b) Characterization Techniques

3.6 Complex Impedance Analysis

In order to understand the various electro chemical processes occurring in a cell, solid electrolytes are modeled as a combination of resistance, capacitance etc. Since dc conductivity of the electrolyte is important from the point of view of applications, to obtain dc resistance, dc measurement can't be done because of polarization at the electrode/electrolyte interface.

So, complex impedance spectroscopy is a technique to separate the contributions from various processes such as electrode reaction at the electrode/electrolyte interface and the migration of charges through the grains and across grain boundary[28]. In order to extract dc resistance, ac complex impedance spectroscopic technique is employed, where the effect of polarization is avoided. The technique employs the application of small amplitude sinusoidal signal and hence the output signal is compared with that of the input signal to get the impedance modulus and the phase shift corresponding to various circuit elements. This method was first applied to solid electrolytes by Baurle[29].

The complex impedance $Z(\omega)$ at an applied frequency (ω) can be expressed as

$$Z(\omega) = Z_R(\omega) + jZ_I(\omega) \qquad (3.1)$$

or

$$Z(\omega) = Z \exp (j0)$$

where the magnitude of the complex impedance $Z = (Z_I^2 + Z_R^2)^{1/2}$ and $\theta = \text{Tan}^{-1} (Z_I / Z_R)$ is the phase angle. Z_I and Z_R are the Imaginary and real parts of the impedance respectively. The following cases represent the basic configuration.

1) For Pure Resistance

$$Z_R(\omega) = R, Z_I(\omega) = 0$$

Thus the plot of Z_R vs Z_I at various frequencies will be an invariant point.

2) For Pure Capacitor

$$Z_R = 0 ; Z_I = -1/\omega C$$

The complex impedance plot will give a straight line parallel to the negative Z_I axis at $Z_R = 0$.

3) For a Resistance and Capacitor in Series

$$Z(\omega) = R - j/\omega C$$

$$Z_R(\omega) = R; Z_I(\omega) = -1 / \omega C$$

The corresponding plot will be similar to that of case 2 at $Z_R = R$.

4) For Resistance and Capacitance in Parallel

$$Z(\omega) = R (1 / j\omega C) / [R + 1/ (j\omega C)]$$

$$= [R / (1 + \omega^2C^2R^2)] + j [- R^2\omega C / (1 + \omega^2C^2R^2)]$$

$$Z_R = R /(1 + \omega^2C^2R^2); Z_I = - R^2\omega C / (1 + \omega^2C^2R^2)$$

i.e., $$Z_R^2 + Z_I^2 = RZ_R$$

$$(Z_R - R/2)^2 + Z_I^2 = (R/2)^2$$

Which is the equation of a circle of radius R/2 with its center at (R/2,0)

Figs (3.3) and (3.4) show the impedance plots for pure resistor, capacitor and combinations of resistor and capacitors. These plots will be obtained only when non-blocking electrodes are used. When blocking electrodes are used i.e., electrodes of different material other than the solid electrolyte additional interface capacitance come in to picture because of polarization. C_{dl} represents the capacitance at the electrode/electrolyte interface. In this case apart from semicircle a 90^0 line is also obtained for perfectly smooth surfaces.

For polycrystalline materials, grain boundary effect will come in to play. The grains in those materials will offer resistance to the flow of ions. In such a case one can identify another semicircle as shown in Fig.3.4. The bulk resistance in such cases is obtained from the intersection of the semicircle with the real axis in the high frequency region. If we have an increased conductivity at the grain boundaries it will give an apparent resistance which is lower than the bulk.

Another effect which can be seen in some poly-crystalline samples, is the depression of semicircle. i.e., the center of the semi-circle will not lie on the real axis. Instead, it will be slightly lower than that. It has been shown that in this case a constant phase element connected in parallel with the bulk resistance will result in such a spectrum with a depressed semicircle[30,31].

The main advantages of impedance spectroscopy are the relatively simple electrical measurements involved and the detailed analysis of impedance data interms of appropriate model of the electrode-electrolyte system can provide information about electrode reaction, mobility etc and bulk properties of the sample. The disadvantage being the difficulty in unambiguously determining the equivalent circuits.

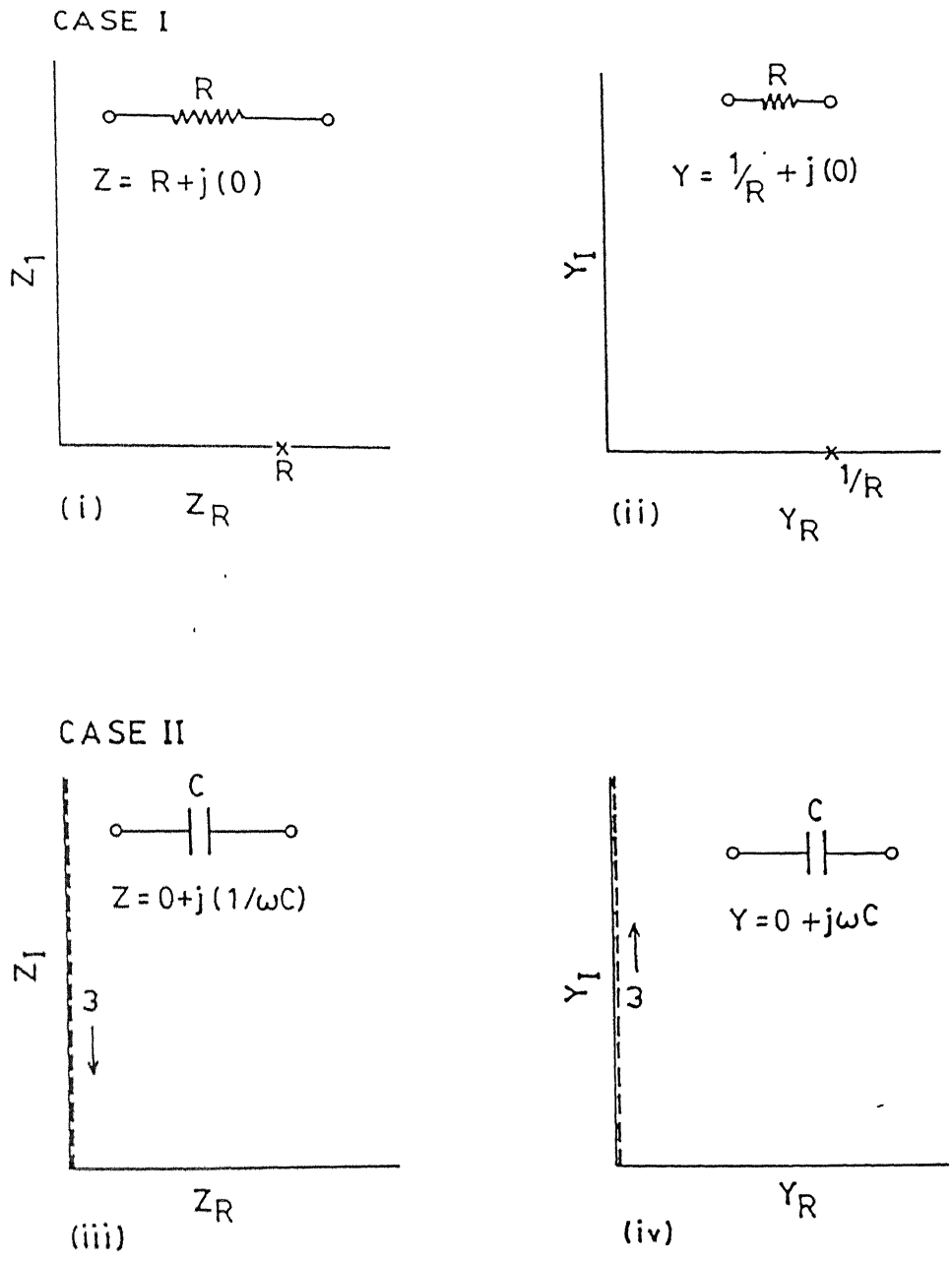

Fig.3.3. Impedance plots for pure resistor and capacitor

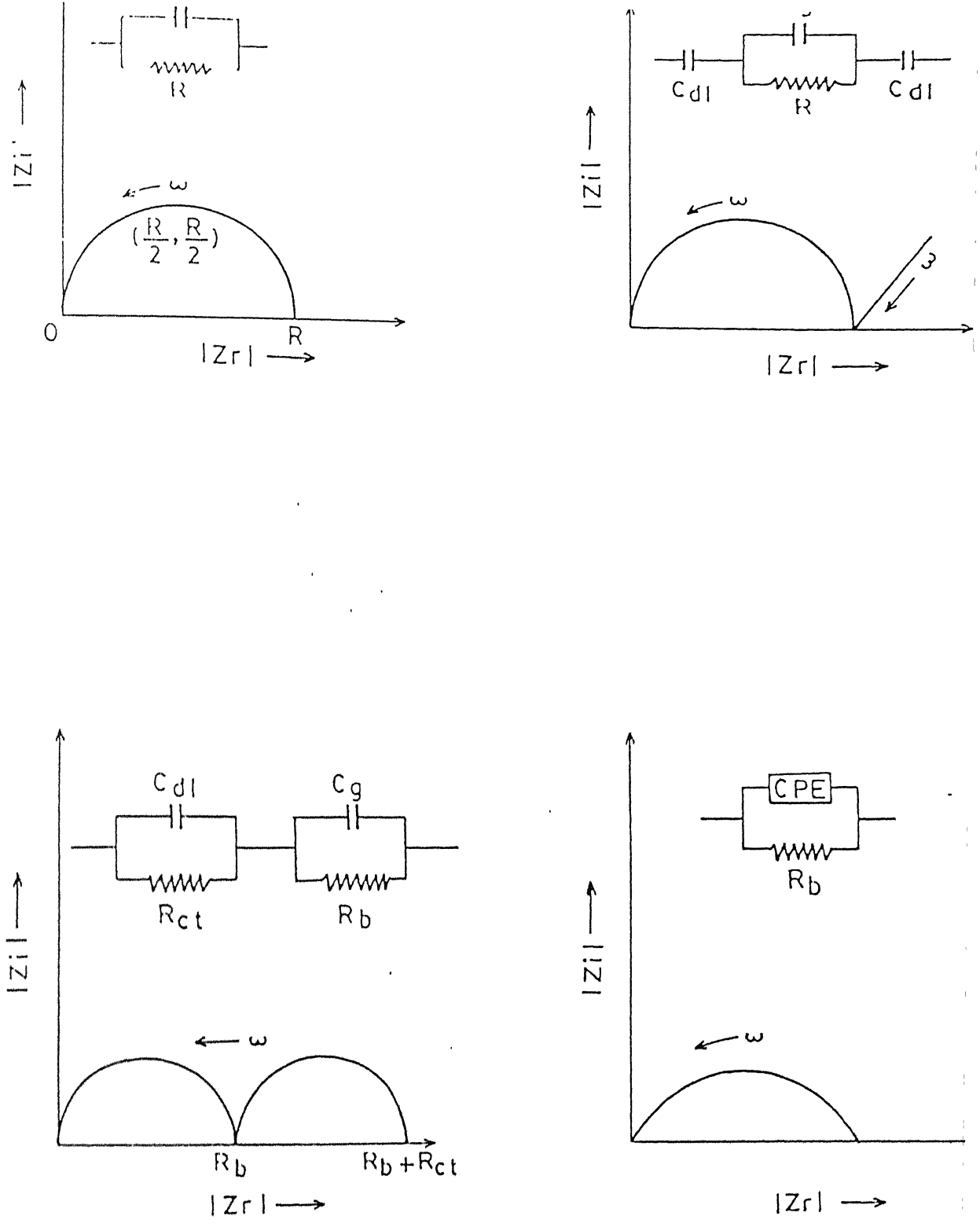

Fig.3.4. Various impedance behaviour observed in solid electrolytes

Fig 3.5 portraits impedance plots for NaCl + 70 m/o LiCl at different temperatures for a range of frequencies from 1 KHz to 10 MHz. The impedance plot consists of | Z cosθ | along x-axis and the | Z sinθ | along y-axis. The diameter of each plot gives the dc resistance of the sample under study. From this the dc conductivity can be calculated using the following expression

$$\sigma_{dc} = l/(R \times A)\ (\Omega^{-1}\ cm^{-1})$$

where l - length of the sample

R - dc resistance of the sample

A - Area of cross section of the sample

It can also be seen that the semicircles are depressed and the center does not lie on the real axis. Whwnever it was not possible to extract dc resistance from the impedance analysis, |Z|/cosθ was taken as resistance and used to calculate ac conductivity.Further, as temperature increases, the diameter of the semicircle decreases.

3.7 X-ray Diffraction of Samples

The X-ray diffraction of all compositions were taken and in Fig.3.6 the XRD patterns of NaCl (pure) to NaCl + 30 m/o LiCl mixed crystals are shown. For NaCl rich sample the peaks are slightly shifted their position and there are no additional peaks. Since the NaCl + x m/o LiCl binary system exhibits a two - phase mixture at room temperature except (20 > x > 80), the XRD patterns should have shown the peaks corresponding to LiCl as well. However, no such peaks were observed, although the peak positions corresponding to NaCl were slightly shifted because of dissolution of some LiCl in NaCl towards higher 2θ values (shrinkage of lattice takes place), implied by Bragg's relation. The absence of LiCl peaks in the NaCl - rich samples may be attributed to the lower concentration of LiCl as well as

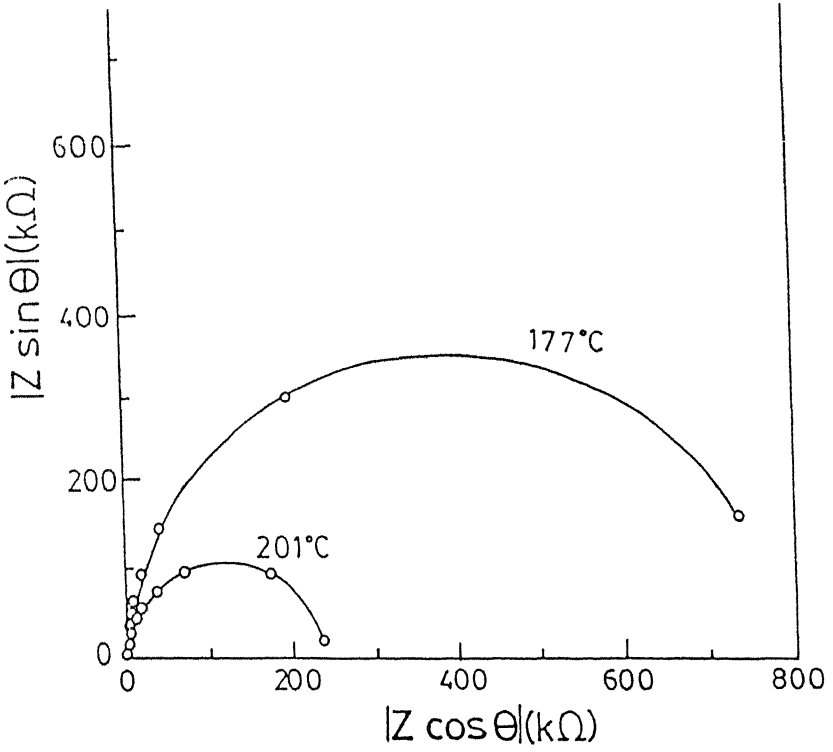

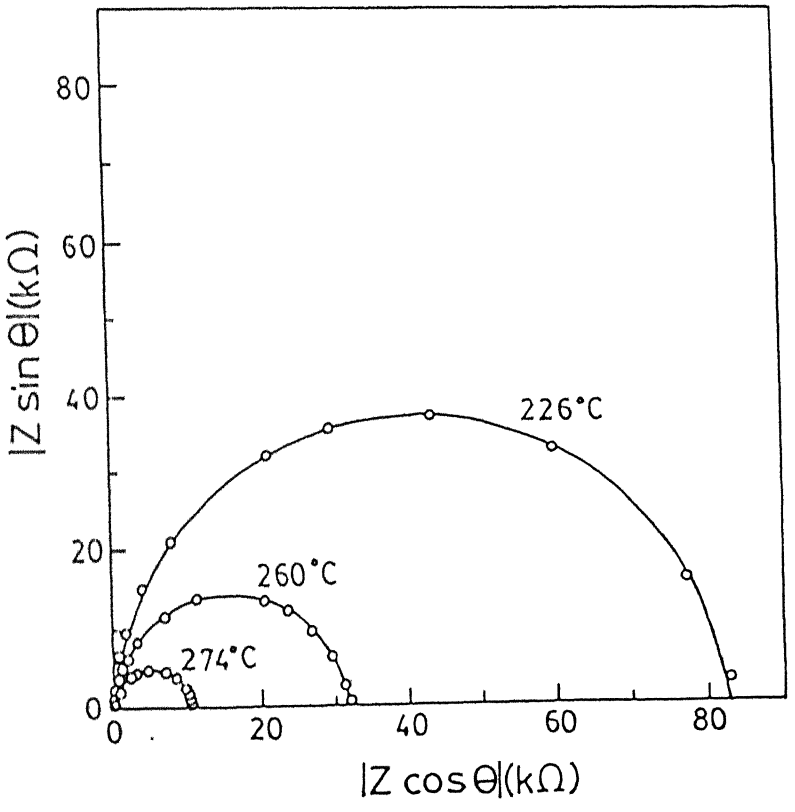

Fig.3.5. Impedance plots for NaCl + 70 m/o LiCl sintered samples

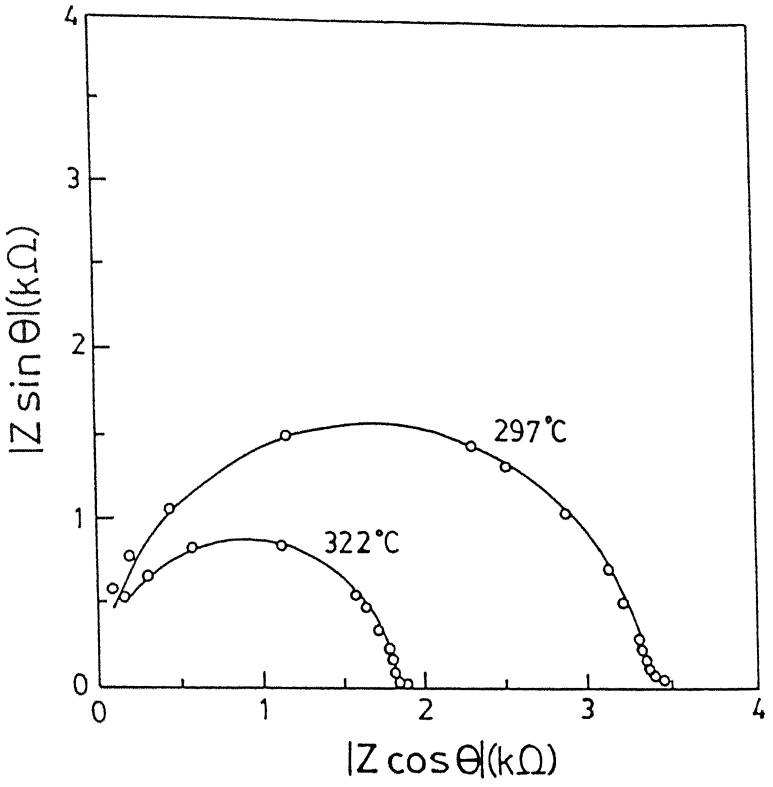
|Z sin θ|(kΩ)
|Z cos θ|(kΩ)
297°C
322°C
0
1
2
3
4

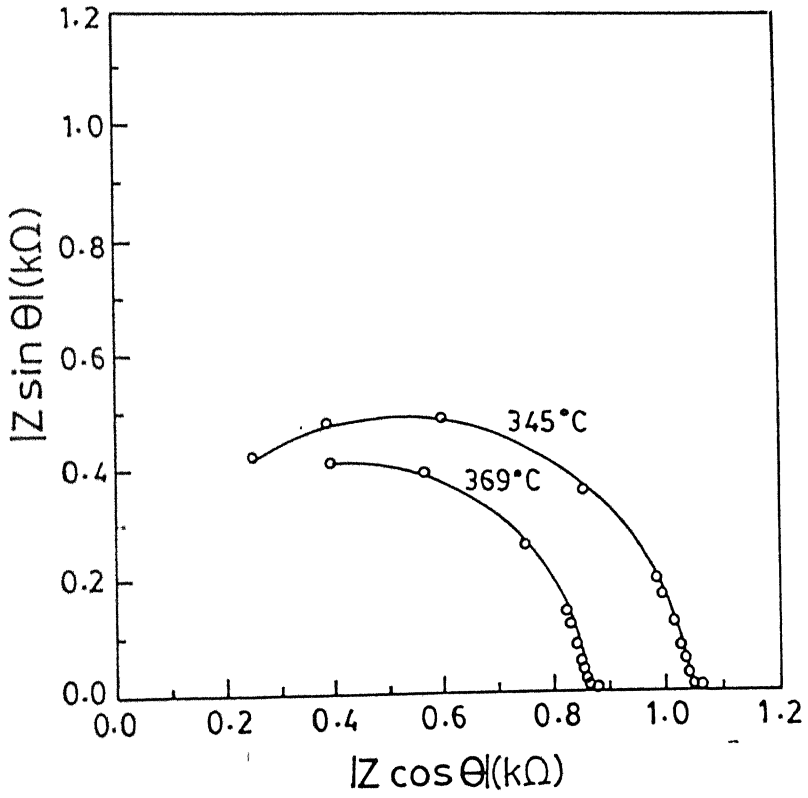
|Z sin θ|(kΩ)
|Z cos θ|(kΩ)
345°C
369°C
0.0
0.2
0.4
0.6
0.8
1.0
1.2

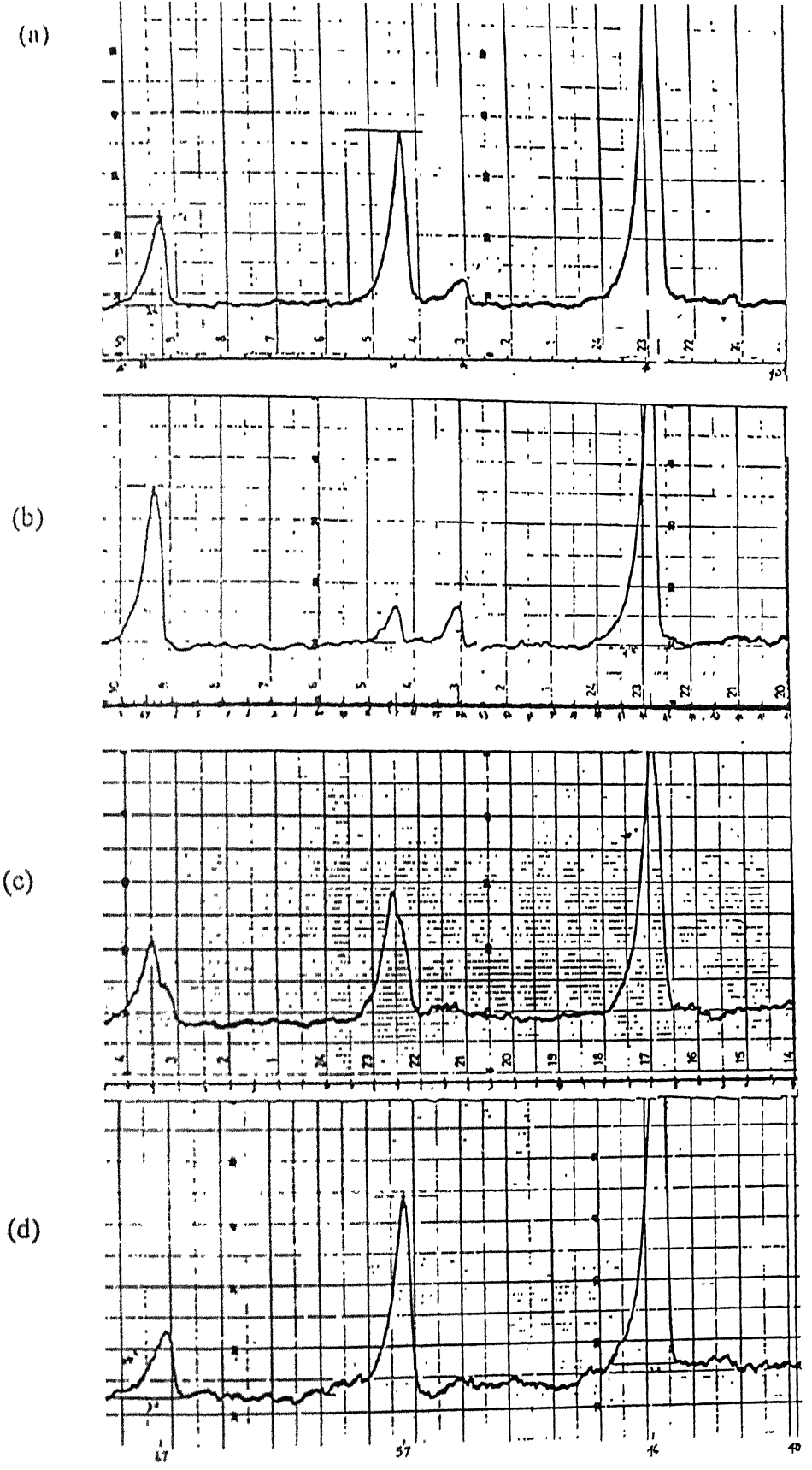

Fig.3.6. XRD pattern of NaCl + x m/o LiCl; (a) x = 0 (b) x = 10 (c) x = 20 (d) x = 30

lower scattering power of smaller Li^+ ions relative to Na^+ ions. Due to hygroscopic nature of LiCl, the XRD patterns of LiCl - rich samples show additional peaks corresponding to hydrates of LiCl. Therefore for LiCl rich samples, very careful XRD measurements, preferably at high temperatures will be desirable

CHAPTER - 4

Results and Discussions

This chapter deals with the experimental results, mainly electrical conductivity, for the NaCl + x m/o LiCl system As pointed out earlier, the aim was primarily to examine the effect of "wrong size" substitutions on the electrical conductivity and also to test the lattice loosening model. In all eleven different compositions of NaCl + x m/o LiCl mixed systems (x = 0, 10, 20, 30 ,40, 50, 60, 70, 80, 90, 100) were prepared and studied. The results on conductivity vs composition are presented followed by the conductivity vs temperature behavior. The XRD results are also already presented in the preceding chapter.

4.1 Ionic conductivity vs composition

Fig.4.1 shows the variation of dc conductivity (σ) as a function of composition (x) for the mixed crystals $Na_{1-x}Li_xCl$ at two different temperatures in the intrinsic region. It may be mentioned that NaCl - LiCl system, according to the available phase - diagram[32], exhibits complete solid solubility only at above ~ 314^{0}C. As evident from Fig.4.1, the σ increases rapidly as the concentration of homovalent Li^+ ions in NaCl increases and attains a maximum value of ~ 1.78×10^{-2} $\Omega^{-1}cm^{-1}$ at 560^{0}C (~ 6.46×10^{-2} Ω^{-1} cm^{-1} at 636^{0}C) at x ≈ 70 m/o LiCl which is about ~ 4×10^3 times larger than that of pure NaCl. As the concentration of LiCl increases further, the σ naturally decreases. As pointed out earlier, LiCl is very hygroscopic which affected the accuracy and reproducibility of the results, especially for LiCl - rich mixed crystals, inspite of our best efforts.

The conductivity vs composition results (Fig.4.1) may be explained by the lattice loosening model[12,16] which suggests that the substitution of either larger or

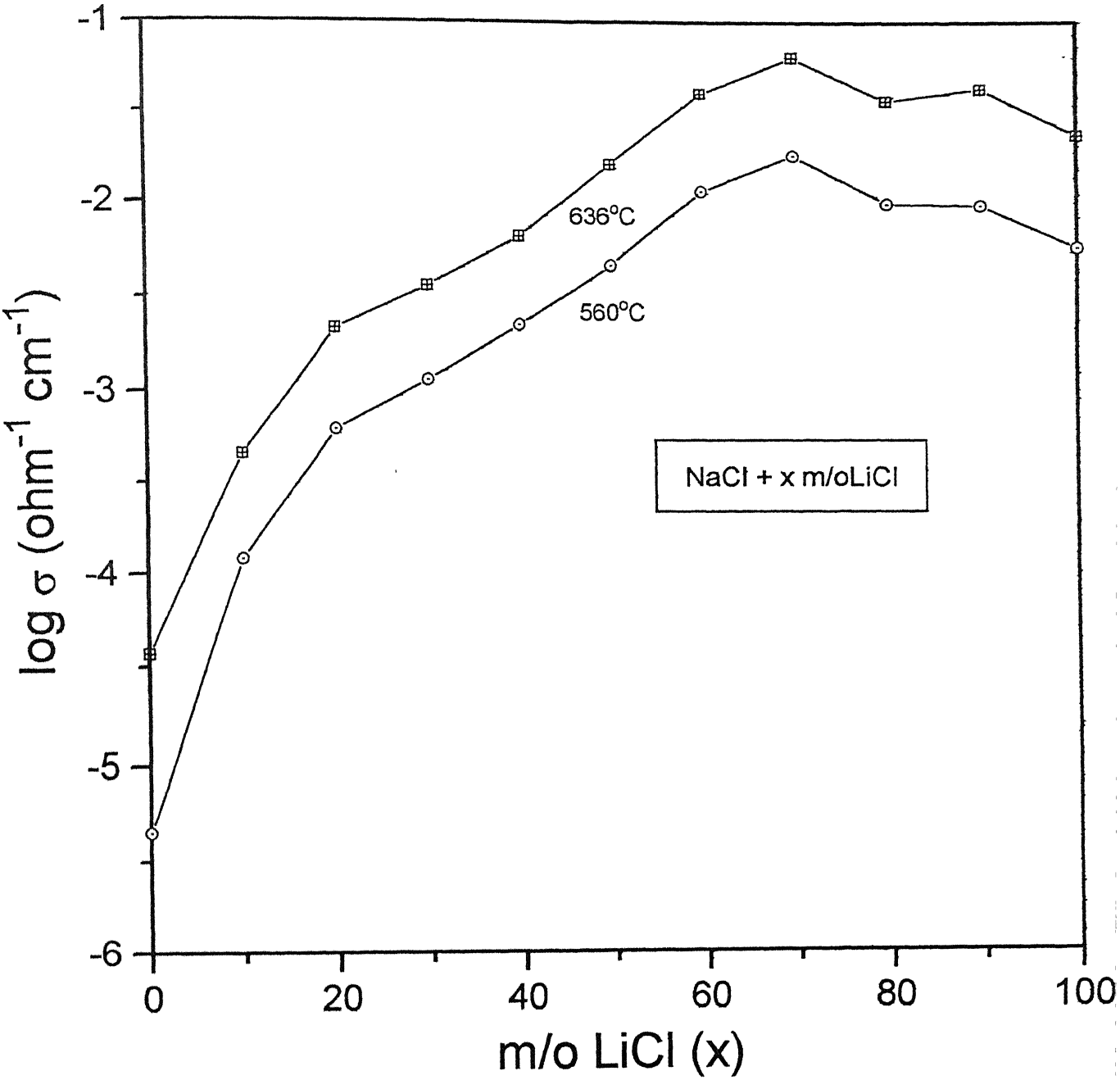

Fig.4.1.Logarithm of conductivity vs concentration of LiCl (x) for NaCl + x m/o LiCl ($0 \leq x \leq 100$) mixed crystals at 560^0 and 630^0C

smaller ions than the host upsets the minimum (stable) energy configuration of the host crystal and thus leads to lattice loosening resulting invariably in decrease in the melting temperature as well as in enthalpies of formation and migration of point defects. Like in most mixed crystal systems studied so far, there is a good correlation between the σ - composition and T_m - composition (phase - diagram) of NaCl - LiCl system as well. It may be noted that the NaCl + 70 m/o LiCl system which exhibits maximum conductivity, has the lowest melting point[32]. A qualitative understanding of the enhancement in the conductivity can be had from the following expression derived from the assumptions of the lattice loosening model [21].

$$\sigma_x / \sigma_0 = \exp [-(\alpha/2 + \beta) \Delta T_m(x) / kT] \qquad (4.1)$$

where α and β are constants, σ_x and σ_0 are the conductivities of mixed crystal and the pure component, $\Delta T_m = T_{mx} - T_{mo}$, where T_{mx} and T_{mo} being the melting temperatures of the mixed crystal and the pure component. For NaCl + x m/o LiCl mixed crystals, the melting temperature $T_m(x)$, may be expressed as

$$T_m(x) = 826 - 7.5\, x + 5.3 \times 10^{-2} x^2 \qquad (4.2)$$

which represents the best fit equation to the experimental solidus curve in the phase diagram[32] shown in Fig.4.2. Combining Eqns (4.1) and (4.2) and substituting the numerical values of $\alpha = 2.14 \times 10^{-3}$ eV/K and $\beta = 0.841 \times 10^{-3}$ eV/K, the expression for relative conductivity for NaCl + x m/o LiCl mixed crystals becomes

$$\sigma_x / \sigma_0 = \exp [\, 22.17 (\, 7.5\, x - 0.053\, x^2) / T] \qquad (4.3)$$

Fig.4.3 compares the experimental values of relative conductivity (σ_x/σ_0) with those calculated from Eq.4.3 at two different temperatures. Evidently, there is a fair agreement between the calculated and the theoretical values as far as the broad features such as the general shape of the curves and appearance of maximum around

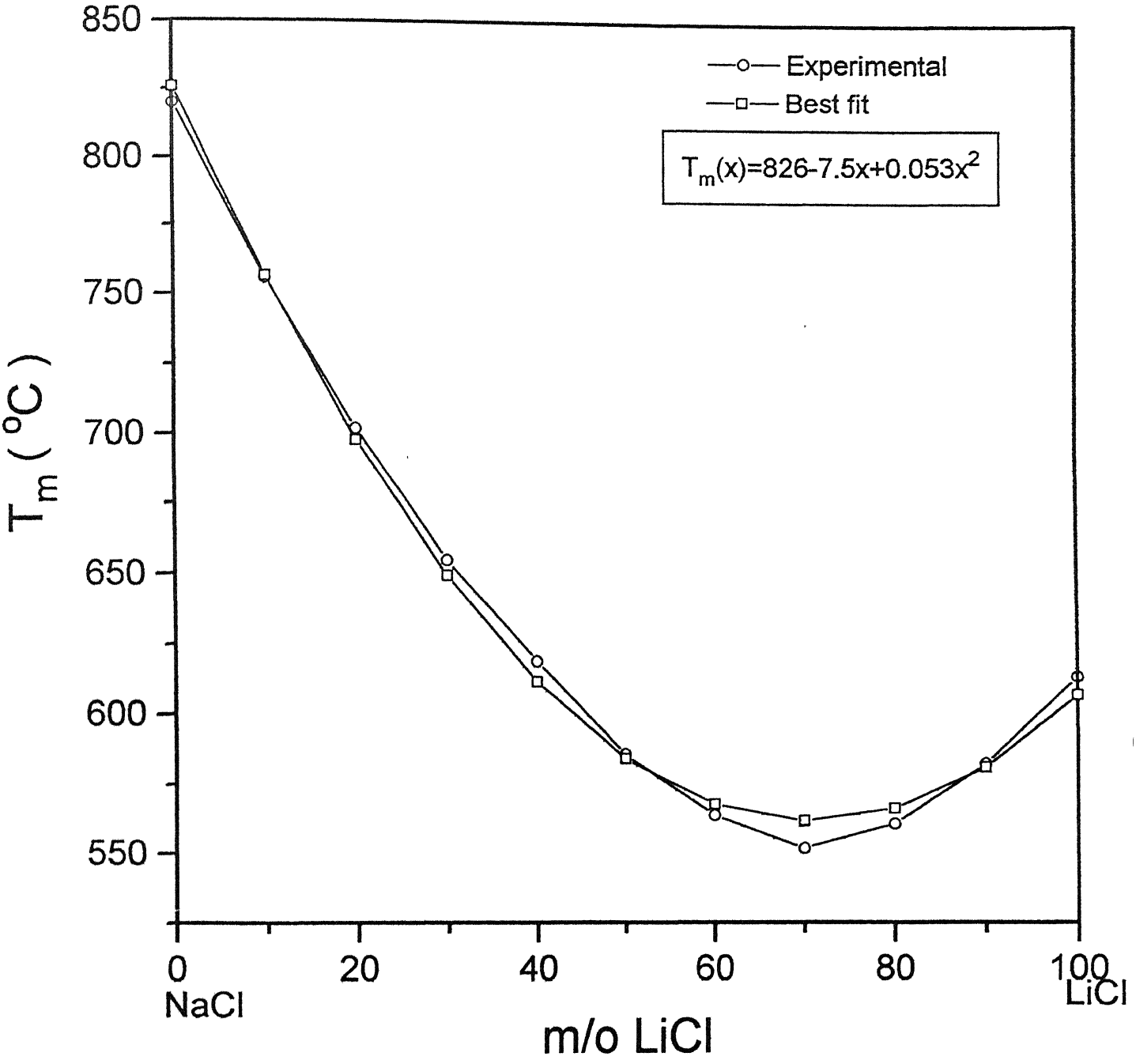

Fig.4.2. Melting temperature (in ^{0}C) vs concentration of LiCl (x) for NaCl + x m/o LiCl ($0 \leq x \leq 100$) mixed crystals. The experimental data is taken from reference 32.

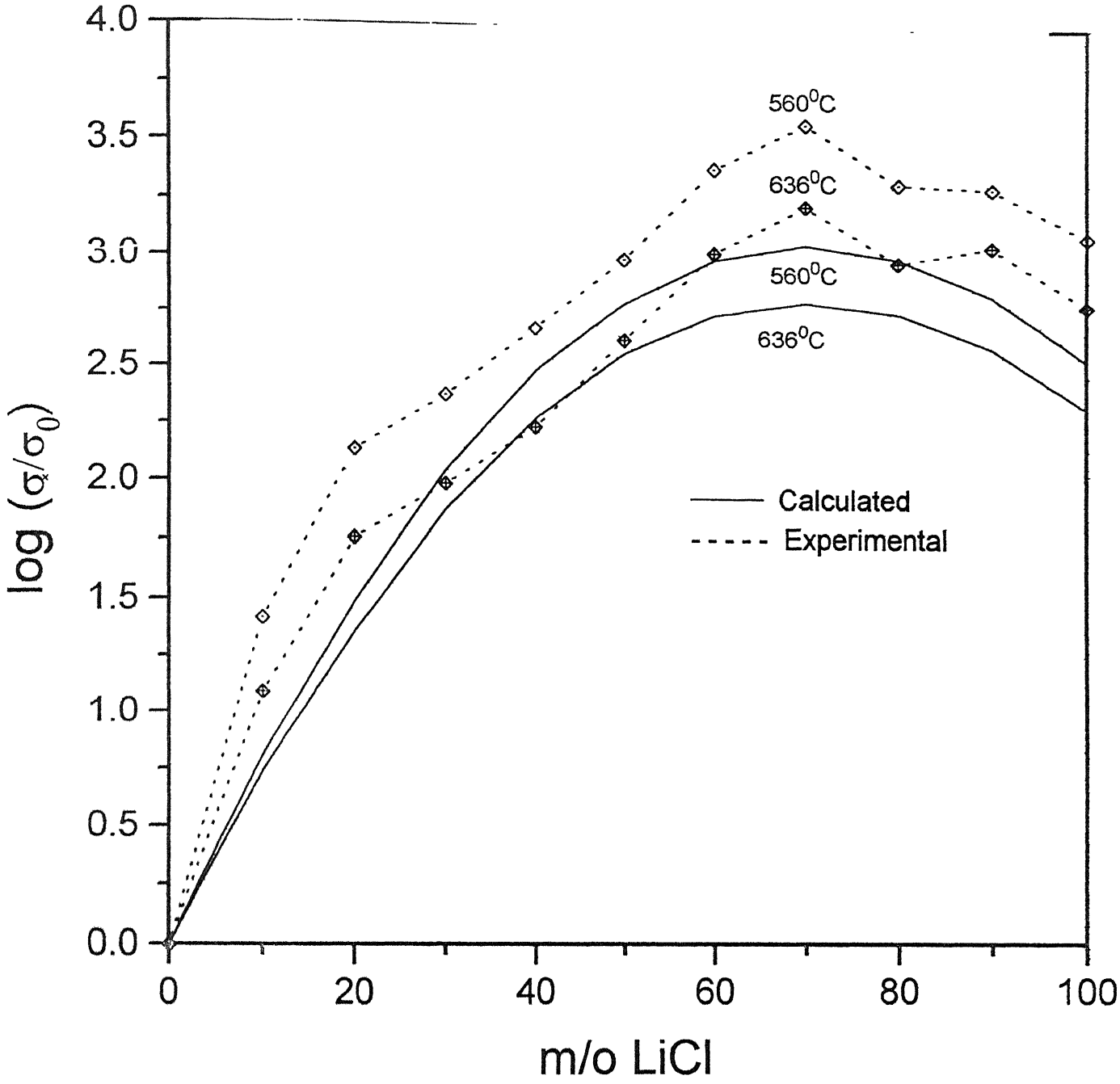

Fig.4.3. Logarithm of relative conductivity (σ_x/σ_0, σ_x and σ_0 being the conductivities of the mixed crystals and pure salt respectively) vs concentration of LiCl (x) in NaCl at 560^0 and 636^0C. The calculated values according to the lattice loosening model are shown by solid lines

70 m/o LiCl are concerned. However, the calculated values of σ_x/σ_0 are generally lower than the experimental values and the discrepancy between the two results is larger at lower concentrations of the LiCl. It may be pointed out here that both the (relative) conductivity and the melting point are much more sensitive to the concentration (x) of the homovalent dopants initially (at lower values of x). Since the lattice loosening model (Eqns.4.1 and 4.3) critically depends on the melting temperature vs composition data, an accurate measurement of the latter is important. The available phase diagram data (Eqn.4.2) is too old and it may be advisable to reinvestigate.

Lattice loosening model can also be tested by comparing the theoretical and experimental values of temperature (T_σ ^{0}K) at which various compositions attain the same conductivity (constant σ). The value of conductivity is fixed in the intrinsic range of conductivity vs temperature (Fig.4.5 and 4.6) plots for different mixed crystals (experimental value). The theoretical and experimental values of T_σ (^{0}K) obtained for NaCl + x m/o LiCl ($0 \leq x \leq 100$) are plotted against the concentration of LiCl (x) in Fig.4.4 for $\sigma = 10^{-3}$ and $10^{-2.75}$ Ω^{-1} cm^{-1}. The preexponential factor (A) is taken to be 10^{+4} Ω^{-1} cm^{-1}. Since A varies from 10^{+3} to 10^{+5} Ω^{-1} cm^{-1} for different mixed crystals and pure component the above mentioned mean value is taken.

The theoretical value of T_σ is obtained as follows. The conductivity of mixed crystals is given by

$$\sigma_x = A_x \exp [- (H_{sx} / 2 + H_{mx}) / kT] \qquad (4.4)$$

where A_x is the preexponential factor of mixed crystal and other terms have their usual meaning corresponding to mixed crystals. Eqns.2.33 and 2.40 relate the formation and

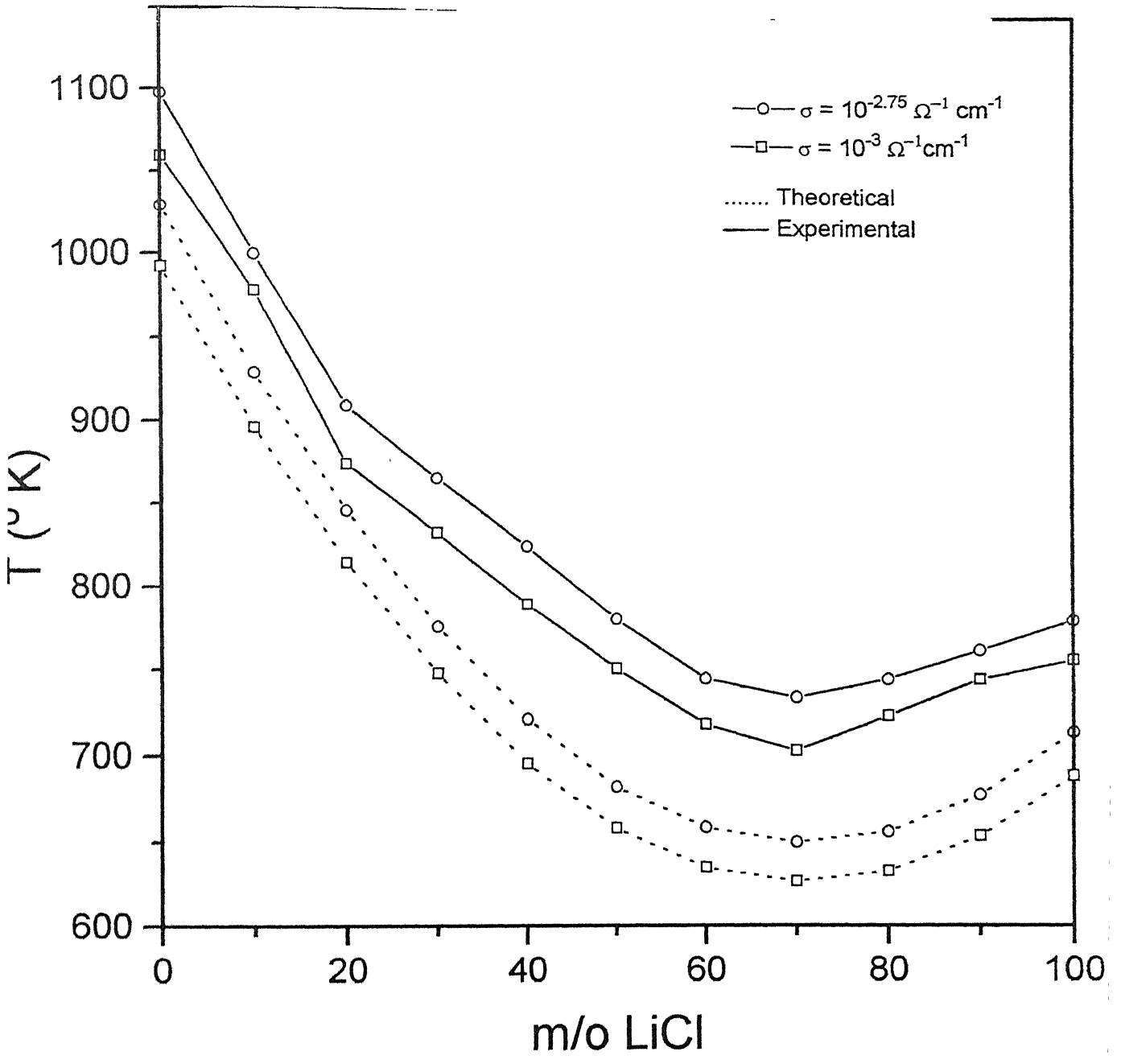

Fig.4.4. Isoconductivity plots for NaCl + x m/o LiCl ($0 \leq x \leq 100$) mixed crystals

migration enthalpies to the melting point of the mixed crystals. Thus using those eqns, eqn 4.4 becomes

$$\sigma_x / A_x = \exp \{ - (\alpha /2 + \beta) T_{mx} + \gamma / kT \} \qquad (4.5)$$

since σ_x is the same as that of pure components, it is denoted as σ i.e., $\sigma_x = \sigma$. Further, the dopant concentration do not affect the preexponential factor i.e., $A_x = A$ is almost constant[21] for all composition.

From Eqn.4.5, we get,

$$T_\sigma = [- (\alpha / 2 + \beta) T_{mx} + \gamma] / k \ln (\sigma / A) \qquad (4.6)$$

From the above expression it is evident that a variation of $10^{\pm1}$ or $10^{\pm2}$ in A will not seriously affect T_σ since the expression contains logarithmic dependence of A. Since α, β, γ, σ and A ($10^{+4}\ \Omega^{-1}\ cm^{-1}$) are constant T_σ depends on T_{mx} which is obtained from the best fit equation for the solidus curve of Fig.4.2. Thus T_σ should follow T_{mx}.

In Fig.4.4, the experimental data corresponding to the above mentioned fixed conductivities are taken from the log σ vs 10^3 / T studies discussed in the next section. The variation of T_σ is surprisingly similar to that of T_{mx}. Both T_σ vs composition (x) plots exhibit a minimum at $\approx$ 70 m/o LiCl similar to that of T_{mx} vs composition (x) plot.

In brief, eqn.4.6 provides yet another way to test the lattice loosening model (LL model) and the close agreement between the nature of T_σ vs x and T_{mx} vs x curves would suggest that the LL model for explaining the enhanced ionic conductivity in mixed crystals is quite satisfactory.

4.2 Conductivity vs Temperature

The variation of logσ as a function of the inverse temperature for the NaCl + x m/o LiCl mixed crystals is shown in Fig.4.5 ($x \leq 40$ m/o) and Fig.4.6 ($x \geq 70$ m/o

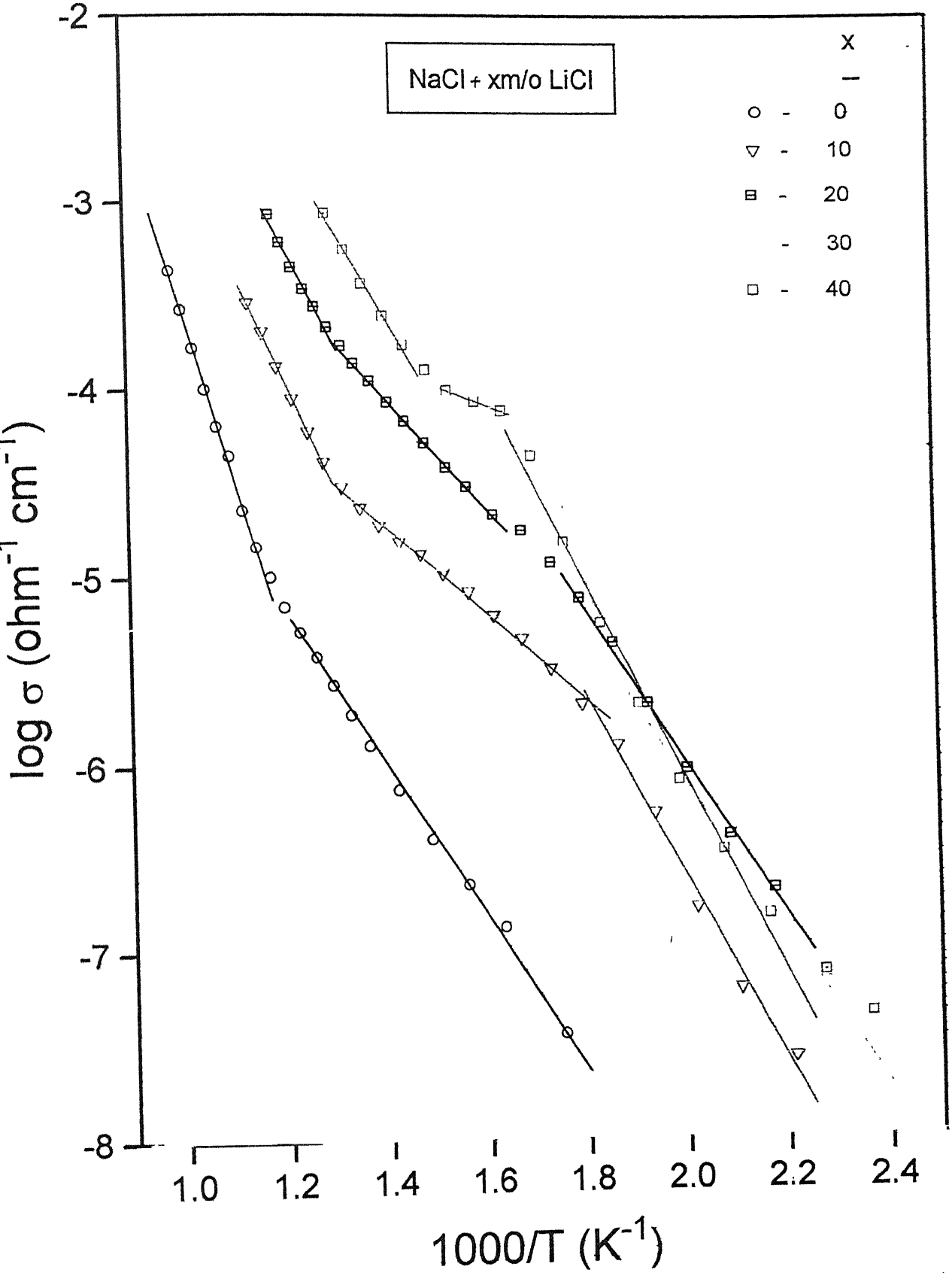

Fig.4.5. Logarithm of conductivity vs inverse of temperature (1000/T, K^{-1}) for NaCl + x m/o LiCl ($0 \leqslant x \leqslant 40$) mixed crystals

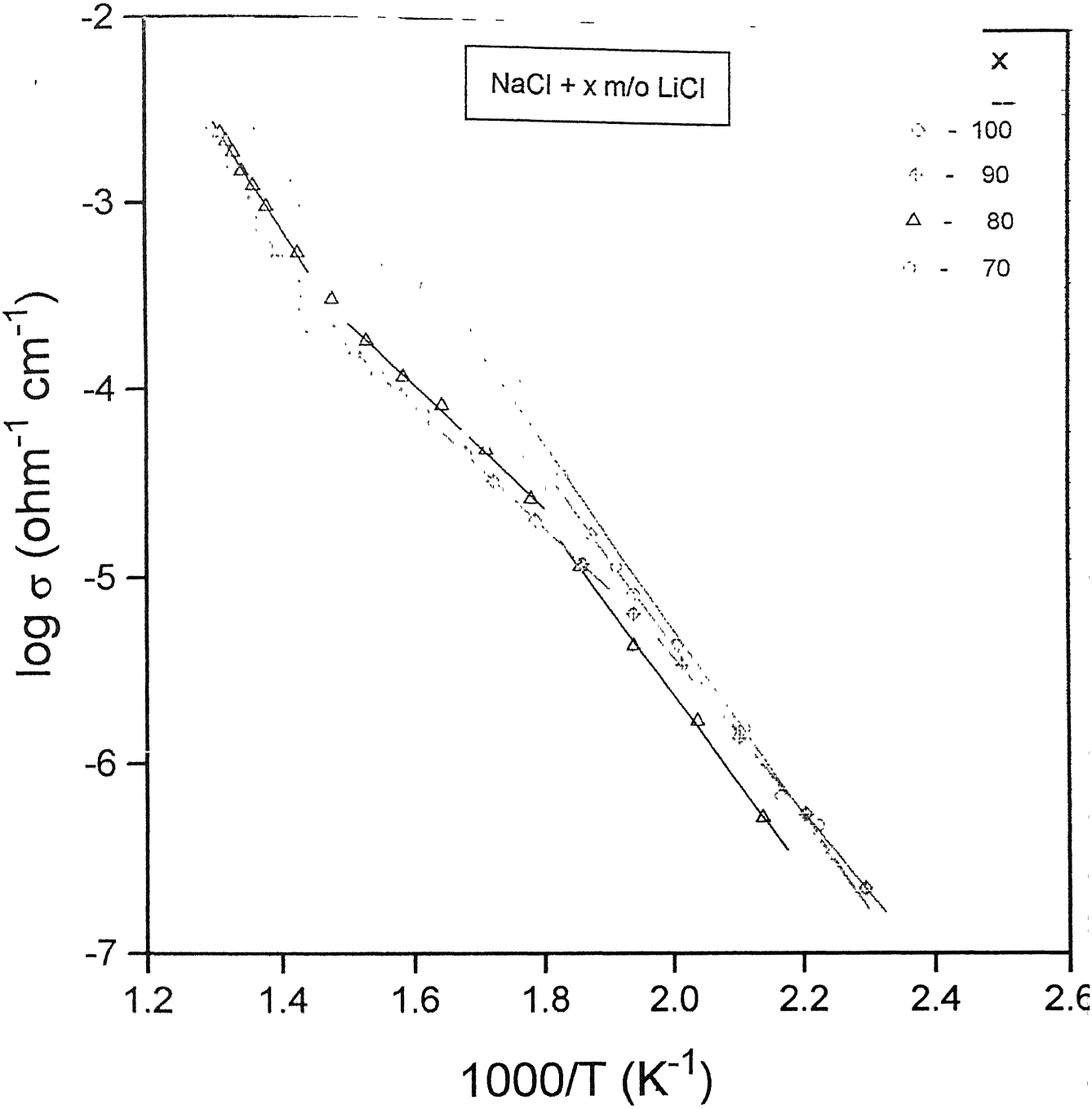

Fig.4.6. Logarithm of conductivity vs temperature (10^3/T, K^{-1}) for NaCl + x m/o LiCl ($70 \leq x \leq 100$) mixed crystals

). Alkali halides normally exhibit two linear regions in logσ vs 1000/T plots. Thus our results for pure NaCl are consistent with earlier findings. However, our results for pure LiCl, hence also LiCl-rich mixed crystals, exhibit three distinct regions; high temperature intrinsic region as usual but two extrinsic regions which may be labeled as region-2 and region-3 (lowest temperature region).

4.2.1 Intrinsic Region

For all compositions the logσ vs 10^3/T plots are found to obey the Arrhenius equation

$$\sigma = A \exp(- E_a / kT) \qquad (4.7)$$

where A is the preexponential factor and E_a the activation energy (eV). From NaCl (pure) to NaCl + 70 m/o LiCl there is a clear enhancement in σ, which exactly follows the phase diagram as the melting temperature decreases from pure NaCl to 70 m/o LiCl. Similarly for LiCl to LiCl + 30 m/o NaCl, there is a clear enhancement in the conductivity. Fig.4.7 depicts the activation energy vs composition. The activation energies corresponding to LiCl rich mixed crystals do not quite follow the phase diagram. Since the conductivity of NaCl + 70 m/o LiCl is maximum, its activation energy should have been minimum but the observed results (Fig.4.7) exhibit a minimum around 40 m/o LiCl. As pointed out earlier, the measurements on LiCl-rich samples were far less reproducible.

4.2.2 Region 2 and Region 3

Fig.4.6 shows three linear regions for pure polycrystalline LiCl. The origin of region 2 may be related to the divalent impurities already present in LiCl. It is also known that the presence of CO_3^{2-} ions causes large deviation in the slope of the extrinsic region in KI[5] crystal. Hence it is suspected that there may be a possibility of

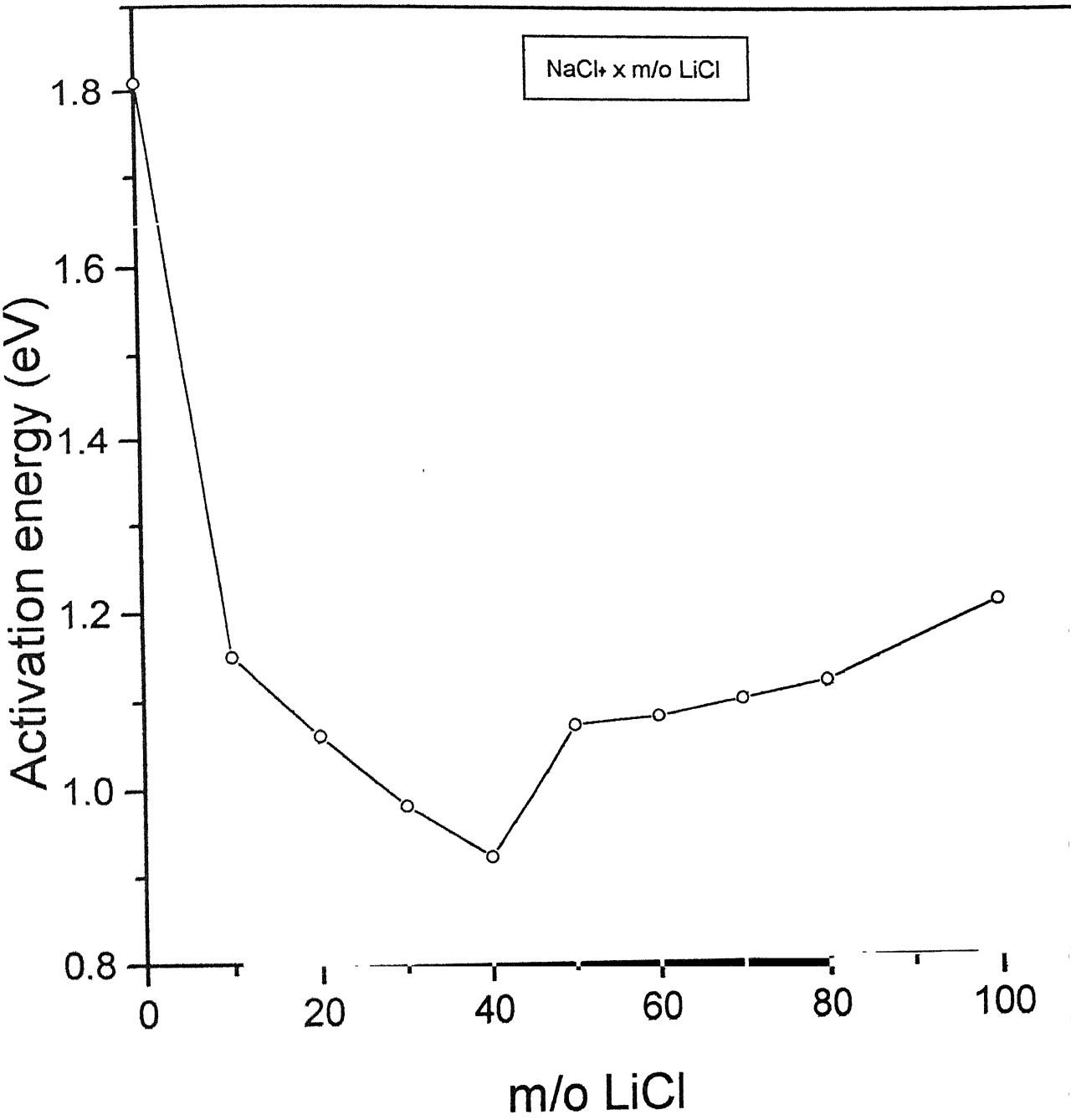

Fig.4.7. Activation energy vs concentration of LiCl (x) for NaCl + x m/o L
($0 \leq x \leq 100$) mixed crystals

presence of carbonate ion in LiCl. If this divalent impurity is uniformly present, then the slope of region-2 should decrease uniformly for increased composition of LiCl. An inspection of the Table 3 will reveal that there is no uniformity in the variation of slopes.

It is well known that the divalent cation/anion impurities may form an association with the compensating charged vacancies at lower temperatures. Such impurity-vacancy pairs are neutral and do not contribute to the conductivity. As a result the conductivity begins to decrease much faster as temperature decreases in this so called extrinsic associated region[14]. It may be noticed in Fig 4.5 and 4.6 that almost all solid solutions, except pure NaCl, exhibit three linear regions in their logσ vs $10^3/T$ plots. The lowest temperature region can thus be identified as extrinsic associated region. The interpretation of conductivity behavior in this region, for certain compositions, becomes more complicated because of separation of two phases, viz., NaCl solid solution (NaCl ss) and LiCl (ss) which is further discussed below.

4.2.3 Precipitation of second phase particles

In Fig.4.5, it may be noticed that the NaCl + 30 m/o LiCl sample exhibits a strange behavior at intermediate temperatures(i.e., region - 2). As temperature decreases, the σ at a certain intermediate temperatures starts increasing first before resuming a normal course. This unusual behavior may be attributed to the precipitation of second phase particles leading to composite effect[13] as also observed in KBr - NaI system[21]. When the precipitation is complete, the conductivity decreases rapidly as expected. Thus the initial enhancement in σ in this region is because of precipitation of LiCl solid solution (LiClss) which may be considered to be dispersed in the NaClss matrix. The nucleation and grain growth of the two phases viz. LiClss and NaClss

Table 3. Conductivity at 560° and 636°C, Preexponential factor (A), Activation energy (E_a in eV) of NaCl + x m/o LiCl ($0 \leq x \leq 100$)

Material	Temperature range * (°C)	Preexponential factor (A) (Ω^{-1} cm^{-1})	σ at 560°C (Ω^{-1} cm^{-1})	σ at 636°C (Ω^{-1} cm^{-1})	Activation energy E_a (eV)
NaCl (Pure)	740-600	3.98×10^{5}	4.57×10^{-6}	3.71×10^{-5}	1.81
	580-300				0.82
NaCl+10m/o LiCl	605-505	1.07×10^{3}	1.20×10^{-4}	4.57×10^{-4}	1.15
	466-284				0.46
	263-180				0.98
NaCl+20m/o LiCl	575-500	1.58×10^{3}	6.3×10^{-4}	2.14×10^{-3}	1.06
	470-345				0.57
	303-187				0.82
NaCl+30m/o LiCl	540-420	0.98×10^{3}	1.1×10^{-3}	3.63×10^{-3}	0.98
	380-275				-
	250-145				0.82
NaCl+40m/o LiCl	500-420	0.81×10^{3}	2.2×10^{-3}	6.46×10^{-3}	0.92
	380-335				-
	315-190				1.05
NaCl+50m/o LiCl	520-395	1.35×10^{4}	4.57×10^{-3}	1.59×10^{-2}	1.07
	360-285				0.53
	240-165				0.85
NaCl+60m/o LiCl	490-425	3.89×10^{4}	1.15×10^{-2}	3.98×10^{-2}	1.08
	410-360				0.58
	325-180				0.88
NaCl+70m/o LiCl	500-430	8.13×10^{4}	1.78×10^{-2}	6.46×10^{-2}	1.10
	390-345				0.36
	295-175				0.98
NaCl+80m/o LiCl	490-430	5.89×10^{4}	1.00×10^{-2}	3.63×10^{-2}	1.12
	385-290				0.64
	265-195				0.94
NaCl+90m/o LiCl	495-430	5.25×10^{5}	9.55×10^{-3}	4.27×10^{-2}	1.28
	405-265				0.21
	225-165				0.59
LiCl (Pure)	550-415	1.17×10^{5}	5.75×10^{-3}	2.29×10^{-2}	1.21
	365-295				0.31
	260-173				0.93

* logσ vs $10^3/T$ plots, for the mixed crystals, consist of three distinct regions. The intermediate and low temperature regions are referred to as region- 2 and region- 3 in the text.

from the parent phase helps one to understand this phenomenon. It should be pointed out that at any temperature $T < T_c$, the rate and growth of phase separation will be proportional to the

1) Temperature difference (T_e - T) where T_e is the equilibrium temperature at which the three phases LiClss, NaClss and LiCl (NaCl) + x m/o NaCl (LiCl) coexist. It is ~ 419^0C for 30 m/o LiCl. The conductivity is maximum at 356^0C for the same composition.

2) The diffusion coefficient D of the ions in the parent phase. $D \propto \exp (- G / kT)$, where G is the free energy of diffusion. As the temperature decreases, (T_e - T) increases and hence the rate of phase separation will increase. However, on decreasing the temperature, the diffusion coefficient (D) affects the rate of phase separation. A state appears for which any increase in T_e - T will cause D to become dominant and the conductivity falls down i.e., any further phase separation is hampered.

4.3 Conclusions

The substitution of homovalent (Li^+) ions in NaCl enhances the conductivity considerably; the conductivity of NaCl + 70 m/o LiCl is approximately 4 $\times 10^3$ times higher than that of pure NaCl at 560^0C. The mismatch between the sizes of the dopant and the host ions obviously plays a dominant role in the enhancement of conductivity. The lattice loosening model explains satisfactorily the conductivity enhancement in the intrinsic region for all compositions of the present system but it may be desirable to determine T_m vs x more accurately. The enhancement in the conductivity of the two phase mixture at the lower temperatures suggests the possibility of dispersion less composite solid electrolytes.

REFERENCES

1) T. Kudo / K. Fueki (1990) Solid State Ionics, Kodansh Ltd., Tokyo (Japan)

2) K. Shahi and J.B Wagner.,Jr (1981) J. Electrochem Soc. **128**, 6

3) K. Shahi and J.B. Wagner.,Jr (1981) Phys. Rev. **B12**, 6417

4) S. Geller (1977) Solid Electrolytes, (Ed.S.Geller), Springer-Verlag, Berlin

5) S. Chandra (1981) SuperIonic Solids, North-Holland Publishing Company, Amsterdam

6) R.J. Friauf (1972) In Physics Of Electrolytes (Ed.J. Hladik), vol-1, Academic Press, New York, London

7) C.C.Liang (1973) J.Electrochem.Soc.**120**, 1289

8) A.C. Khandkar and J.B. Wagner.,Jr (1986) Solid State Ionics **20**, 267

9) K. Shahi and J.B. Wagner.,Jr (1982) J. Solid State Chem.**42**, 107

10) T. Jow and J.B. Wagner.,Jr (1975) J. Electrochem Soc.**126**, 1963

11) J.B. Holt, H.G. Sockel and H. Schmalzried (1969) J. Am. Ceram. Soc. **52**, 375

12) K. Shahi and J.B. wagner.,Jr (1983) J. Phys. Chem. Solids **44**, 89

13) S.Gupta, S. Patnaick, S. Chaklanobis and K. Shahi (1988) Solid State Ionics **31**,5

14) T. Bhima Sankaram and K.G. Bansigir (1978) Crystal Lattice Defects **7**, 209

15) A. Schiraldi, E. Pezzati and G. Chiodelli (1978) Z. Physik. Chem. neue folge **110**,1 as cited by P. Manoravi in his Ph.d thesis (1991)

16) K. Shahi and J.B. Wagner.,Jr (1982) J. Phys. Chem. Solids **43**, 713

17) K. Shahi and J.B. Wagner.,Jr (1982) J. Solid State Chemistry **42**, 107

18) S. Ihara, Y. Warita and K. Suzuki (1984) Phys. Stat. Solidi (a) **86**, 729

19) R. Mercier, M.Tachz, J.P. Malguani and G. Robert (1985) Solid State Ionics **15**,109

20) V.N. Erofeev and E. Hartmann (1988) Solid State Ionics **28**, 241

21) P. Manoravi and K. Shahi (1991) J. Phys. Chem. Solids **52**, 527

22) O. Johannesan and M. Mckelvy (1986) J. Phys. Chem. Solids **47**, 265

23) O. Johannessen (1987) Proc. of the 6th Int. Conf. on Solid State Ionics, p.1310

24) P. Manoravi (1991) Ph.D Thesis, I.I.T. Kanpur

25) P. Manoravi and K. Shahi (1991) Solid State Ionics **45**, 83

26) L.W. Barr and A.B. Lidiard (1970) In Physical Chemistry - An advanced treatise, Academic press, New York

27) L.W. Barr and D.K. Dawson (1971) Proc. Britt. Ceramic. Soc **19**, 151 as cited by P. Manoravi in his Ph.D thesis

28) R. Macdonald (1987) Impedance Spectroscopy, John Wiley and Sons

29) J.E. Bauerle (1969) J. Phys. Chem. Solids **30**, 2657

30) J. Ross Macdonald (1984) Solid State Ionics **13**, 147

31) I.D. Raistrick (1986) Solid State Ionics **18**, 40

32) Phase Diagram for Ceramists (1964) (Ed. M.K. Resser) Am. Ceram. Soc., Columbus, Ohio.

Publications / Presentations

1. " Wrong Size Effect in NaCl - LiCl Mixed Crystals " by B.T.S. Ramanujam and K. Shahi - presented at Condensed Matter Physics Symposium held at I.I.T. Kanpur in February, 2000.
2. " Wrong Size Effect in NaCl - LiCl Mixed Crystals" by B.T.S. Ramanujam and K. Shahi - presented at Fourth National Conference in Solid State Ionics held at I.I.T. Bombay from 3-5 march, 2000; Paper to be published in Mats.Res.Bulletin, Bangalore.